LETTERS
https://doi.org/10.1038/s41477-021-00922-0

nature plants

Transcriptional and imprinting complexity in *Arabidopsis* seeds at single-nucleus resolution

Colette L. Picard[1,2], Rebecca A. Povilus[1], Ben P. Williams[1] and Mary Gehring[1,3] ✉

Seeds are a key life cycle stage for many plants. Seeds are also the basis of agriculture and the primary source of calories consumed by humans[1]. Here, we employ single-nucleus RNA-sequencing to generate a transcriptional atlas of developing *Arabidopsis thaliana* seeds, with a focus on endosperm. Endosperm, the primary site of gene imprinting in flowering plants, mediates the relationship between the maternal parent and the embryo[2]. We identify transcriptionally uncharacterized nuclei types in the chalazal endosperm, which interfaces with maternal tissue for nutrient unloading[3,4]. We demonstrate that the extent of parental bias of maternally expressed imprinted genes varies with cell-cycle phase, and that imprinting of paternally expressed imprinted genes is strongest in chalazal endosperm. Thus, imprinting is spatially and temporally heterogeneous. Increased paternal expression in the chalazal region suggests that parental conflict, which is proposed to drive imprinting evolution, is fiercest at the boundary between filial and maternal tissues.

Flowering plant seeds are complex structures, comprising a diploid maternally derived seed coat that surrounds two products of distinct fertilization events: the embryo and endosperm. The diploid embryo represents the next generation of the plant. The endosperm is an often-triploid tissue (due to the presence of an additional maternal genome complement) and is an altruistic mediator of the relationship between its sibling embryo and their resource-supplying mother. Endosperm is a key evolutionary innovation of flowering plants and has been identified as the site of genomic imprinting, an epigenetic gene-regulatory process that results in differential expression of maternally and paternally inherited alleles[1,2]. Although an ephemeral tissue, endosperm undergoes a unique developmental programme that includes differentiation into three morphologically and spatially defined domains: the micropylar domain surrounds the embryo, the chalazal domain occupies the opposite end of the seed, and the peripheral domain lies in between[3–8]. Gene-expression patterns in the three endosperm domains have been assessed by microarray analysis[9], but it is unknown whether cell-type heterogeneity exists within domains. Despite its evolutionary and agronomic importance, endosperm biology remains relatively little understood. A complete record of all transcriptionally unique cell or nuclei types within the endosperm has been unobtainable owing to the compact, interconnected and complex nature of seeds.

To build a comprehensive map of transcriptional complexity and to examine imprinting dynamics during early endosperm development in *Arabidopsis*, we performed single-nucleus RNA-sequencing (snRNA-seq). We isolated nuclei instead of cells because the endosperm is syncytial during its early development and organized into nucleocytoplasmic domains[5–8]. Later, endosperm undergoes progressive cellularization in a wave from the micropylar to chalazal pole[5–8]. We obtained high-quality transcriptomes for 1,437 nuclei using fluorescence-activated sorting of 4,6-diamidino-2-phenylindole (DAPI)-stained seed nuclei (FANS) to enrich for 3C or 6C endosperm nuclei, using a modified Smart-Seq2 protocol[10] for library preparation (Fig. 1a, Extended Data Fig. 1, Supplementary Figs. 1 and 2 and Supplementary Data 1). On average, we detected expression from 3,200 genes per 3C endosperm nucleus and 4,200 genes per 6C endosperm nucleus (Supplementary Fig. 1). We clustered all snRNA-seq data using the SC3 program[11], obtaining 27 clusters ranging in size from 8 to 172 nuclei (Extended Data Fig. 2). Based on initial clustering and the fraction of maternal allele expression per nucleus, we identified 966 endosperm nuclei, 464 seed-coat nuclei and 7 embryo nuclei (Extended Data Figs. 1 and 2, Supplementary Data 1 and Supplementary Material). Although we assayed multiple time points and genotypes, most profiled nuclei (74%) were from F_1 seed from reciprocal crosses between the wild-type strains Col and Cvi obtained at 4 days after pollination (DAP) (Fig. 1a and Supplementary Data 1) and were the focus of subsequent analyses.

To test whether our clustering strategy reliably identified distinct cell or nuclei types, we took advantage of the 356 seed-coat nuclei collected at 4 DAP (Extended Data Fig. 1 and Supplementary Data 1). The seed coat has at least five distinct cell layers and two major domains (general and chalazal)[9,12]. Our nuclei clustering yielded six clusters for Col-derived seed coat (from Col × Cvi crosses) and eight clusters for Cvi-derived seed coat (from Cvi × Col crosses) (Extended Data Fig. 3). To assign putative identities to the computationally defined clusters, we evaluated the expression of genes known to be expressed in specific seed-coat cell layers and also performed Gene Ontology (GO) term enrichment analysis on differentially expressed genes (Extended Data Figs. 3 and 4, Supplementary Figs. 3–5 and Supplementary Data 2). Our clustering and characterization corresponded well with known seed-coat cell types and provides the first whole-genome expression data set for distinct layers and regions of the seed coat (Extended Data Fig. 3 and Supplementary Material).

We next applied our analysis method to the 802 endosperm nuclei isolated from Col–Cvi endosperm at 4 DAP. A single *Arabidopsis* seed has ~350 endosperm nuclei at the stage assayed[13], so this data set should represent a near complete sampling. We identified 14 distinct nuclei clusters in Col × Cvi F_1 endosperm (CxV E1–E14) and 11 clusters in Cvi × Col (VxC E1–E11) (Fig. 1b), suggesting there is previously undescribed transcriptional heterogeneity within the three known endosperm domains. We determined the identity of endosperm clusters by: evaluating the expression of known marker genes for micropylar, peripheral and chalazal endosperm; differential gene expression and GO term enrichment analysis; in situ hybridization for cluster-specific transcripts;

[1]Whitehead Institute for Biomedical Research, Cambridge, MA, USA. [2]Computational and Systems Biology Graduate Program, Massachusetts Institute of Technology, Cambridge, MA, USA. [3]Department of Biology, Massachusetts Institute of Technology, Cambridge, MA, USA. ✉e-mail: mgehring@wi.mit.edu

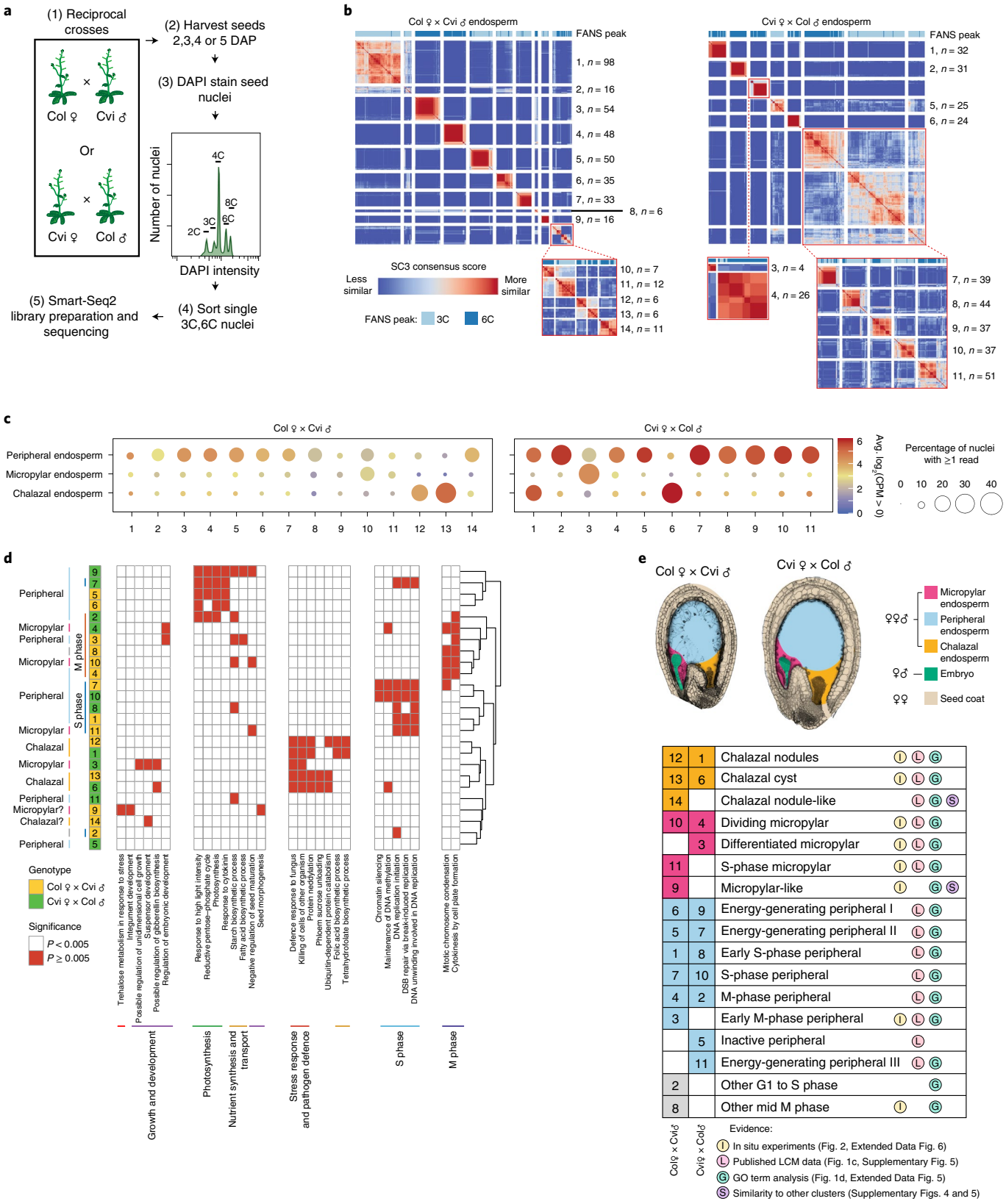

Fig. 1 | Distinct nuclei types in *Arabidopsis* endosperm. a, Overview of experimental approach. **b**, SC3 clustering of Col × Cvi and Cvi × Col 4 DAP endosperm nuclei. Insets: reclustering to further resolve distinct groups. **c**, Average expression of marker genes for peripheral, micropylar and chalazal endosperm regions, based on refs. [9,52]. **d**, Heatmap of a subset of significantly enriched GO terms among genes upregulated in each cluster. **e**, Seed images at 4 DAP, with seed regions false-coloured, and identification of the nuclei states corresponding to each cluster. DSB, double-strand break; LCM, laser-capture microdissection.

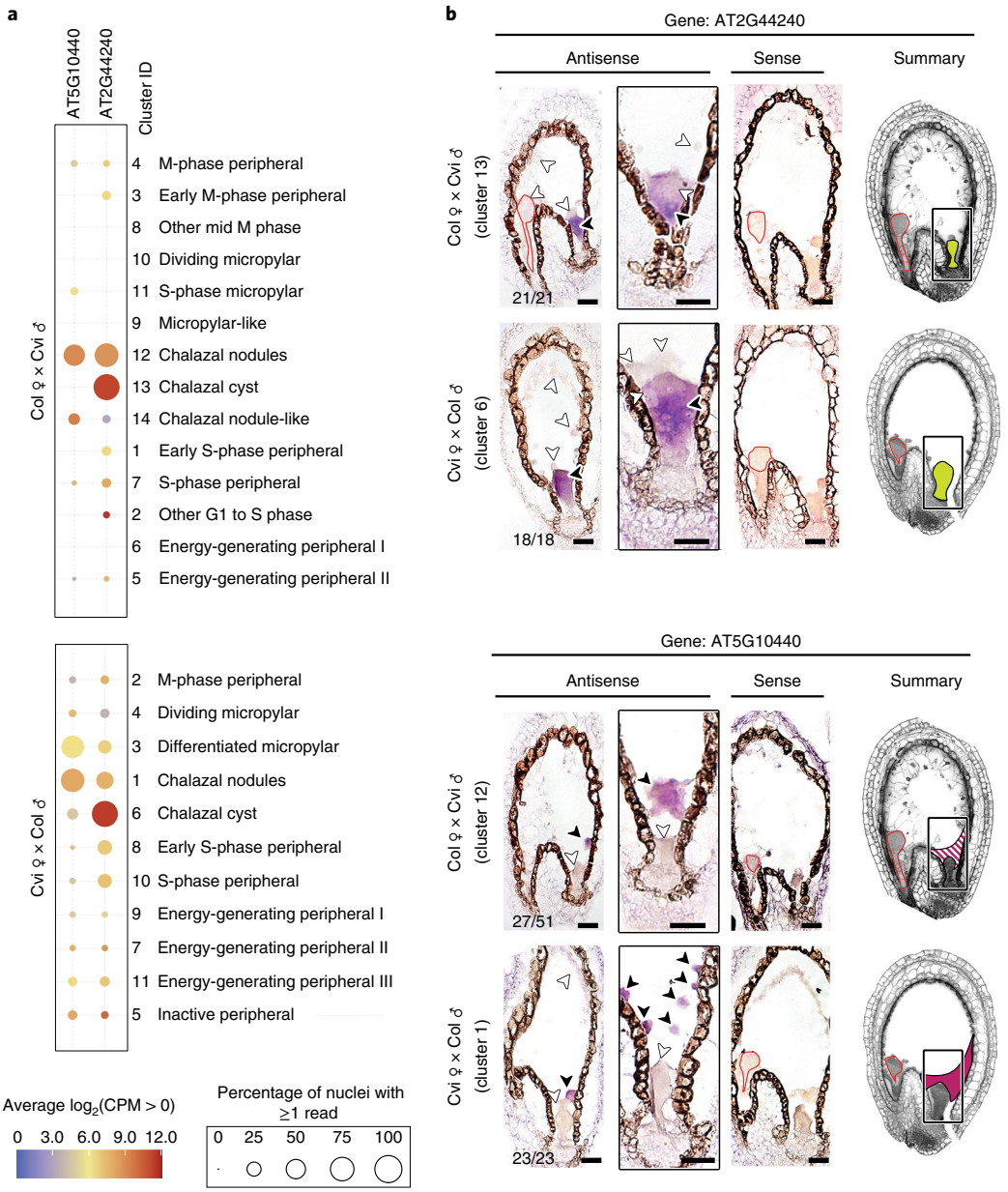

Fig. 2 | Identification of clusters by in situ hybridization analysis. a, Average expression of two chalazal endosperm cluster-specific genes selected for in situ hybridization. **b**, RNA in situ hybridization (purple signal) in 4 DAP seeds. Black arrowheads, transcript detected; white arrowheads, no transcript detected. Embryos outlined in red. Number of seeds with the pictured expression pattern, as well as total number of seeds observed, indicated in the bottom left of each image. Images without numbers represent higher magnification images or images of sense probes. False-coloured images summarize gene-expression patterns for each locus and cross direction. Solid colours, consistent detection; striped pattern, variably detected. Scale bars, 25 µm. Seeds were from three independent controlled pollination events, collected together. For all antisense probes, an in situ experiment was performed at least twice.

and cell-cycle trajectory analysis. We identified several endosperm clusters corresponding to micropylar and peripheral endosperm nuclei, some related to cell-cycle phase differences and others to putative functional differences (Figs. 1c–e and 2, Extended Data Figs. 5–7, Supplementary Figs. 4–7, Supplementary Material and Supplementary Data 2 and 3).

Gene expression analysis and the overlap of known endosperm domain markers suggested that at least two distinct clusters in each genotype corresponded to chalazal endosperm, which is thought to be a primary site of nutrient transfer between the mother and offspring[4] (Fig. 1c,d and Supplementary Figs. 4 and 5). Anatomically, the chalazal endosperm consists of two regions, nodules and the cyst. The chalazal nodules are large, possibly multinucleate bodies lining the chalazal region[4,14], whereas the chalazal cyst is a cytoplasmically dense, multinucleate region that forms at the interface between the endosperm and adjacent maternal tissue[4,15]. Whether nodules or cysts have distinct functions or transcriptional profiles is largely unknown[6], although a handful of differences in gene expression have been described[16,17]. We performed RNA in situ hybridization on marker genes expressed specifically in the putative chalazal endosperm clusters (Fig. 2 and Extended Data Fig. 6). These experiments showed that two transcripts most highly expressed in CxV E12 and VxC E1, AT5G10440 and AT1G44090, were localized specifically to the chalazal nodules (Fig. 2 and Extended Data Fig. 6).

In contrast, AT2G44240 and AT4G13380, which are primarily expressed in CxV E13 and VxC E6, were detected only in the chalazal cyst (Fig. 2 and Extended Data Fig. 6). We concluded that the clusters CxV E12 and VxC E1 correspond to the chalazal nodules, whereas CxV E13 and VxC E6 correspond to the cyst (Figs. 1e and 2b). Remarkably, despite the lack of cell membranes and walls in chalazal endosperm, physically adjacent nodule and cyst nucleocytoplasmic domains did not share expression of cluster-specific genes (Fig. 2b). These data are the first transcriptomic description of these cell/nuclei types, providing a basis for further understanding of their developmental and functional differences.

Cell-cycle phase further distinguished the chalazal cyst and nodules. Chalazal endosperm nuclei as a whole were predominantly in G1, G1/S, S and G2, but rarely in M phase, suggesting they undergo endoreduplication (Extended Data Fig. 7, Supplementary Fig. 6 and Supplementary Data 3). This is consistent with observations that chalazal endosperm nuclei are larger than other endosperm nuclei and likely polyploid[8,15], and with our finding that chalazal nuclei were preferentially sorted from the 6C FANS peak (Fig. 1b). More than half of nodule nuclei were in G1/S or S phase, while most cyst nuclei were in G1 or G2 (Extended Data Fig. 7). No M-phase nuclei were detected in the chalazal cyst. Thus, the cyst consists primarily of nuclei that are non-dividing or that spend little time in S phase.

All chalazal clusters showed high expression of genes related to pathogen defence and cell killing, as well as protein neddylation (Fig. 1d and Extended Data Fig. 5). Additionally, genes highly expressed in chalazal nodules were involved in tetrahydrofolate and folic acid biosynthesis, a key step in one-carbon metabolism and a major target process for crop biofortification[18]. By contrast, the cyst was enriched for ubiquitin-dependent protein catabolism and phloem sucrose unloading (Fig. 1d and Extended Data Fig. 5). The chalazal cyst is adjacent to the termination of maternal phloem tissue in the chalazal seed-coat region, and the enrichment of genes related to phloem sucrose unloading is consistent with a nutrient transfer function for the cyst. Taken together, these experiments provide the strongest evidence to date that chalazal endosperm likely consists of two spatially, developmentally and transcriptionally distinct nuclei types. These results also suggest that our clustering and characterization approach is both robust and sensitive enough to identify real, biologically distinct groups comprising as few as six nuclei (Fig. 1b).

We next took advantage of the allele-specific nature of our data to examine imprinted expression across the endosperm nuclei clusters we defined. Investigation of parental bias in endosperm allele-specific bulk mRNA-seq data sets[19–24] demonstrates that, whereas imprinted genes are, by definition, significantly biased toward expression from either the maternal or paternal allele, few are expressed exclusively from one allele. Partial imprinting could result from incomplete silencing of the non-expressed allele throughout the endosperm or from heterogeneous imprinting among individual cells or cell/nuclei types. Understanding whether endosperm imprinting is heterogeneous is important for understanding both the cellular and physiological function of imprinting and its underlying epigenetic basis.

We developed a novel analysis framework for evaluating imprinting from snRNA-seq data and one that is suitable for situations in which maternal (m) and paternal (p) allelic dosage is not 1:1 (endosperm is 2m:1p) (Supplementary Figs. 8 and 9, Extended Data Fig. 8 and Supplementary Material). Of 35,366 annotated loci, we were able to assess imprinting for approximately 15,800 genes. We detected significant maternal bias for 357 genes and paternal bias for 110 genes, many of which were previously identified as imprinted genes (Supplementary Figs. 10–12, Supplementary Data 4). Maternally- and paternally-expressed imprinted genes (MEGs and PEGs, respectively) were defined as strong, medium or weak based on the extent of parental bias (Supplementary Figs. 10 and 11 and Supplementary Data 4). Imprinted genes were enriched for similar GO categories as described previously[20], including genes involved in chromatin silencing and regulation of transcription for PEGs (Supplementary Fig. 11).

To determine whether imprinted genes were preferentially expressed in specific nuclei types within endosperm, we examined total and allelic expression patterns across endosperm clusters. MEG expression was not enriched in any specific endosperm nuclei type, with a few exceptions for individual genes (Supplementary Fig. 13). By contrast, nearly half of the PEGs had strongly enriched expression in the chalazal endosperm clusters (Fig. 3a,b, Supplementary Fig. 13 and Supplementary Data 4 and 5). A subset of these was specifically enriched in the chalazal nodules, while another subset was enriched in the cyst (Fig. 3a, Supplementary Fig. 14 and Supplementary Data 5). We found that the increased expression of PEGs in chalazal endosperm reflected increased expression from the paternal allele only, whereas maternal allele expression remained low and largely unchanging across all endosperm clusters (Fig. 3b,c and Supplementary Fig. 14). This effect was not observed for non-imprinted genes with chalazal endosperm-enriched expression (Supplementary Fig. 15). Thus, the paternal allele of many PEGs becomes specifically upregulated in the chalazal endosperm region. Taken together, these results demonstrate that imprinting is heterogeneous among endosperm cell/nuclei types.

Imprinted gene expression is regulated epigenetically, with DNA methylation and the PRC2 histone mark H3K27me3 playing important roles in regulating differential allelic expression[25–27]. We examined the chromatin profile of PEGs in sperm using recently published data[28]. Like unbiased genes, PEGs were enriched for H3K4me3 near the transcriptional start site, suggesting they are transcriptionally active in sperm (Extended Data Fig. 9). We did not identify any striking differences in sperm chromatin profiles between PEGs that were and were not chalazal enriched that might explain their differing behaviour after fertilization (Extended Data Fig. 9). Chalazal endosperm nuclei did, however, show differential expression of known epigenetic regulators (Extended Data Fig. 9). Genes with decreased expression in the chalazal nodule clusters were enriched for the GO term 'regulation of genomic imprinting' due in part to reduced expression of the PRC2 gene *FIE*, the DNA maintenance methyltransferase *MET1* and the 5-methylcytosine DNA glycosylase gene *DME* (Extended Data Figs. 5 and 9 and Supplementary Data 2). Other epigenetic regulators were upregulated, including those that were MEGs and PEGs (Extended Data Fig. 9), some of which were specific to the chalazal cyst, and others that were highly expressed in both nodule and cysts but not in other nuclei types (Extended Data Fig. 9). Some of these epigenetic regulators, such as *MEA*, are known to regulate other imprinted genes in endosperm[25,26]. Although the significance of these findings remains to be established experimentally, we speculate that these factors may be mediating an active parental conflict within the chalazal

Fig. 3 | Imprinting heterogeneity in endosperm. a, A large fraction of PEGs are specifically expressed in chalazal endosperm. Heatmap of total expression ES for all PEGs. **b**, Heatmap of ES (maternal) − ES (paternal), the difference between the allele-specific maternal and paternal expression ES. **c**, Average allelic expression of nuclei in Col × Cvi and Cvi × Col endosperm clusters for two example PEGs, indicated by black arrows in **a** and **b**. Dotted blue line represents simulated expression from two paternal genomes. **d**, Heatmap of total expression ES (left) and maternal (M) and paternal (P) allele-specific ES for S phase (right). Row order is the same for all heatmaps. **e**, Average allelic expression for three MEGs (1–3) that show reduced maternal allele expression in S phase along with one MEG (4) that does not, indicated by black arrows in **d**.

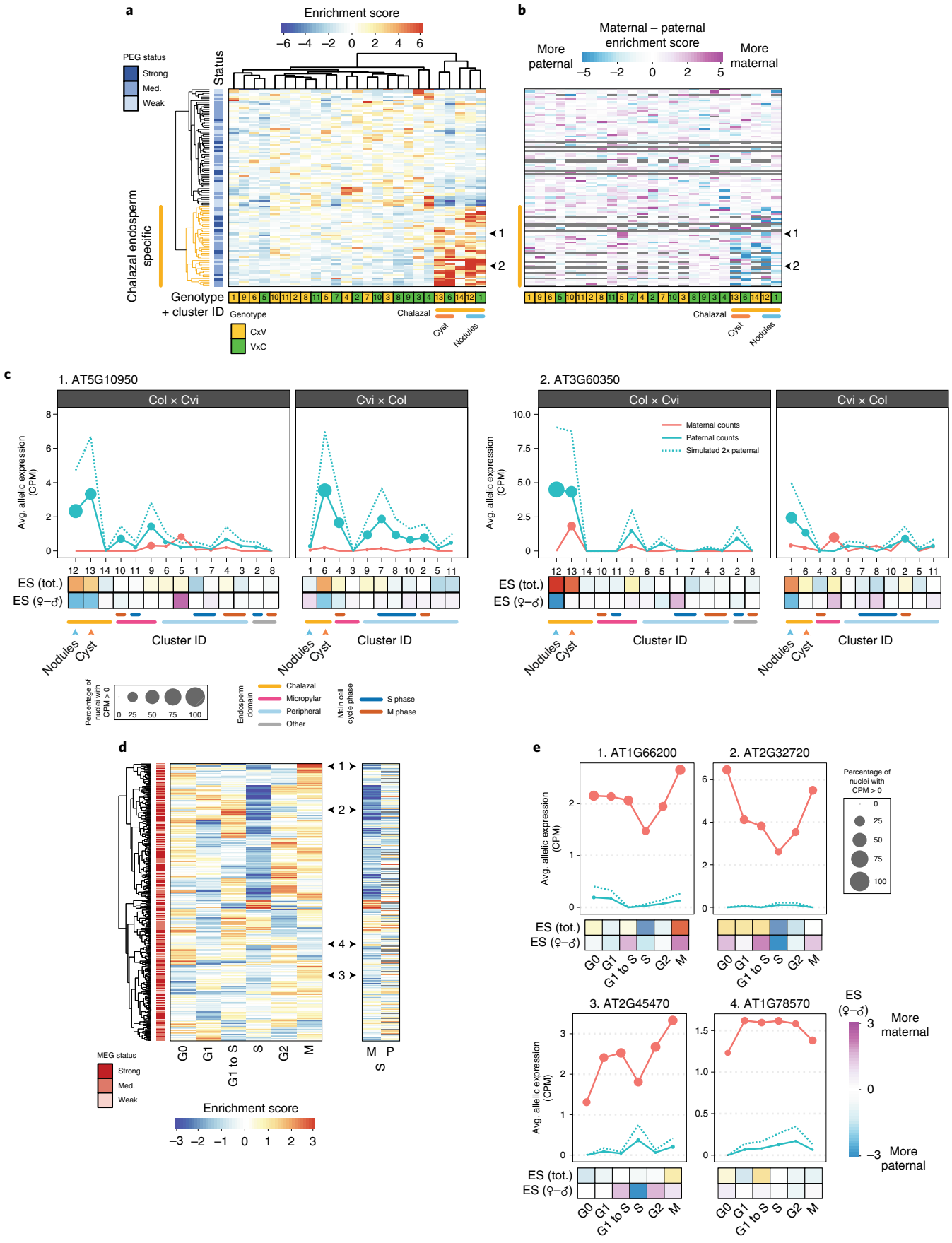
a
Enrichment score
−6 −4 −2 0 2 4 6
PEG status
Strong
Med.
Weak
Status
Chalazal endosperm specific
Genotype + cluster ID
Genotype
CxV
VxC
Chalazal
Cyst
Nodules
1
2
b
Maternal – paternal enrichment score
More paternal
More maternal
−5 −2 0 2 5
c
1. AT5G10950
2. AT3G60350
Col × Cvi
Cvi × Col
Avg. allelic expression (CPM)
Maternal counts
Paternal counts
Simulated 2x paternal
ES (tot.)
ES (♀−♂)
Cluster ID
Nodules
Cyst
Percentage of nuclei with CPM > 0
0 25 50 75 100
Endosperm domain
Chalazal
Micropylar
Peripheral
Other
Main cell cycle phase
S phase
M phase
d
MEG status
Strong
Med.
Weak
G0
G1
G1 to S
S
G2
M
M P
S
Enrichment score
−3 −2 −1 0 1 2 3
e
1. AT1G66200
2. AT2G32720
3. AT2G45470
4. AT1G78570
Avg. allelic expression (CPM)
ES (tot.)
ES (♀−♂)
Percentage of nuclei with CPM > 0
ES (♀−♂)
More maternal
More paternal

endosperm, perhaps by opposing or promoting elevated expression of PEGs. Alternatively, a chalazal endosperm-specific transcription factor could interact with differential maternal and paternal allele epigenetic states to specifically promote expression of the paternal allele of PEGs. Further research is required to determine the molecular mechanism of chalazal endosperm-specific imprinting.

Our data set also allowed us to examine MEG and PEG expression patterns as a function of the cell cycle, which has not been assayed systematically in either mammals or flowering plants. Expression of nearly half of the MEGs identified in our analysis decreased during S phase (Fig. 3d and Supplementary Fig. 16). This pattern was not observed for PEGs or for a set of 500 randomly selected, non-imprinted genes (Supplementary Fig. 16). The lower S-phase expression of MEGs was associated with decreased maternal bias of MEGs, caused by reduced expression of the maternal allele (Fig. 3d,e and Supplementary Fig. 16). During S phase, chromatin states are disrupted and reassembled as DNA is replicated. These data suggest that MEG expression may be particularly sensitive to disruptions in epigenetic state that occur transiently during DNA replication.

We have shown that the endosperm of *A. thaliana* contains a previously undescribed diversity of transcriptionally distinct cell/nuclei types. One important conclusion from this work is that imprinting is dynamic across the cell cycle and/or heterogeneous between cell/nuclei types for a subset of imprinted genes. In particular, many PEGs are most strongly paternally biased in the chalazal endosperm region. This is especially noteworthy in light of the theory that imprinting evolved in flowering plants and mammals as an outcome of conflicts between parental genomes in asymmetrically related offspring over maternal resource transfer[29,30]. The high expression of paternal alleles of PEGs in chalazal endosperm suggests that this conflict is strongest at the interface between maternal and filial tissues in developing seeds. Our study further suggests that fully understanding the regulatory mechanisms underlying imprinting will require approaches specific for a cell/nuclei type. These efforts will aid understanding of epigenetic effects on seed development in other species, including crops.

Methods

Plant material and crossing. All Col-0, L*er* and Cvi-0 plants were grown in a growth chamber (16 h at 22 °C and 120 µm light, 8 h at 20 °C and 0 µm light, 50% relative humidity). Plants were emasculated in the afternoon or evening and pollinated in the morning two days later. FANS was performed in the morning to maximize consistency in seed stage across experiments. However, different crosses developed at different rates: the endosperm of the average CxV F_1 seed (female parent in cross is indicated first) had already begun to cellularize at 4 DAP, whereas VxC F_1 seeds were generally still in the proliferative phase at 4 DAP (Fig. 1e). Embryo developmental stage at 4 DAP was also more variable in CxV crosses, whereas most 4 DAP VxC seeds were at the heart stage (Extended Data Fig. 1). VxC seeds are larger than CxV seeds (Fig. 1e).

RNA in situ hybridizations. Controlled floral pollinations were performed for each cross; more than ten cross-pollinations were performed per cross type. Siliques were harvested at 4 DAP and fixed in formaldehyde, alcohol and acetic acid (10%, 50% and 5%, respectively) overnight at 4 °C. Following dehydration and clearing (HistoClear, National Diagnostics), samples were embedded in Paraplast Plus (McCormick Scientific) with vacuum infiltration and sectioned at 8 µm (Leica RM 2065 rotary microtome). Ribbons were mounted with diethyl pyrocarbonate-treated water on ProbeOn Plus slides (Fisher) at 42 °C and dried overnight at 37 °C. The previously published 602-bp *PDF1* probe was used as a positive control[31]. Experimental probes are listed in the Supplementary Material. Probes were amplified from endosperm cDNA and cloned into TOPO pCR II or TOPO pCR 4 vectors (Thermo Fisher). Plasmids containing sense- and antisense-oriented fragments were identified and linear templates were amplified using M13 forward and reverse primers for probe synthesis. Antisense and sense RNA probes were synthesized in vitro with digoxigenin-UTPs using T7 or SP6 polymerase (DIG RNA Labeling Kit, Roche/Sigma-Aldrich). Probes were then hydrolysed to approximately 300 bp and dot blots were performed to estimate probe concentration. Pre-hybridization steps were preformed according to Jackson[32], except Pronase digestion occurred for 15 min at 37 °C. Hybridization and post-hybridizations were performed according to Bortiri et al.[33], with minor modifications. For higher confidence in directly comparing expression patterns, slides corresponding to the cross and its reciprocal were processed face-to-face in the same pairs for hybridization, antibody and detection steps. Negative controls consisted of hybridizing sense probes. Hybridization was performed overnight at 55 °C, slides were then washed twice in 0.2× saline sodium citrate solution for 60 min each at 55 °C, then twice in NTE buffer (0.5 M sodium chloride, 10 mM Tris(hydroxymethyl)aminomethane hydrochloride, 1 mM ethylenediaminetetraacetic acid, pH 8.0) for 5 min at 37 °C and RNaseA-treated for 20 min at 37 °C, followed by two more washes for 5 min NTE buffer. Slides were incubated at room temperature for 1 h with anti-DIG antibody (Roche/Sigma-Aldrich) diluted 1:1,250 in buffer A (for 500 ml solution: 5 g bovine serum albumin fraction V, 50 ml 1 M Tris(hydroxymethyl)aminomethane hydrochloride pH 7.5, 15 ml 5 M sodium chloride, 1.5 ml TritonX-100, 435 ml water) and then washed four times for 20 min each at room temperature with buffer A and once for 5 min with detection buffer[33]. Colorimetric detections were performed using NBT/BCIP Ready-To-Use Tablets (Roche/Sigma-Aldrich) dissolved in water or BM-Purple (Sigma-Aldrich) with Levamisole (Vector Laboratories). Slides were allowed to develop for 16–46 h before stopping colour precipitation by washing briefly with 50% and then 100% ethanol (NBT/BCIP) or 50% and then 100% methanol (BM-Purple). Slides were mounted in Permount (Electron Microscopy Sciences) and imaged using a Zeiss Axio Imager M2. Colour and brightness/contrast adjustments and Smart Sharpen were applied to whole images, with particular attention to having an even white-balance across different images (Adobe Photoshop).

Seed nuclei FANS. Because the endosperm is a syncytium or only partially cellularized at most of the time points used in this study, and because nuclei transcriptomes are well-correlated with whole-cell transcriptomes[34], we isolated nuclei instead of cells. For FANS, seeds were manually removed from siliques (approximately two siliques per sample) into 50 µl of Partec nuclei extraction buffer (Sysmex) + 6 µl of SUPERase RNase inhibitor (20 U μl^{-1}). Samples were disrupted using a blue pestle in a microfuge tube before adding 400 µl of Partec CyStain UV Precise P nuclei staining buffer and mixing by pipetting. Samples were filtered twice through a 30-µm nylon mesh (Partec CellTrics #04-004-2326, Sysmex). For samples sorted on 12, 13, 20 and 26 September 2018, two additional wash steps were performed to potentially remove cell lysate from the sample (Supplementary Data 1). For each wash, nuclei were spun down for 5 min at 1,000*g* in a centrifuge precooled to 4 °C. Supernatant was then removed and nuclei were gently resuspended in 1 ml of a 1:8 mix of Partec nuclei extraction buffer and Partec nuclei staining buffer. Individual nuclei were sorted into wells of a 96-well polymerase chain reaction (PCR) plate using a BD FACSAria II flow cytometer. A total of 22 full or partial plates (batches) of samples were prepared. Each plate included at least one negative control (no nucleus sorted into well) and one positive control (50 nuclei sorted into a single well) (Supplementary Data 1). Some plates also included wells with two nuclei sorted into each as controls for the precision of single-nuclei sorting. For most sorting experiments, a small number of seeds were separately cleared with a chloral hydrate buffer and imaged to determine developmental stage (Extended Data Fig. 1). Nuclei were sorted from both the putative 3C and 6C peaks based on DAPI fluorescence to enrich for endosperm nuclei (Extended Data Fig. 1 and Supplementary Data 1).

snRNA-seq library preparation and sequencing. FANS samples were prepared at either 2, 3, 4 or 5 DAP. Libraries were prepared according the Smart-Seq2 protocol[10] with a few minor variations and at a reduced volume. Briefly, nuclei were sorted into 1 µl of lysis buffer (0.19% vol/vol Triton-X 100, 2U SUPERase RNase inhibitor, ERCC RNA spike-ins; Thermo Fisher, see Supplementary Data 1). One microlitre of poly(A) hybridization mix (final concentration 2.5 mM/each dNTPs + 2.5 µM oligo(dT) primer) was added to each well and the plate was incubated at 72 °C for 3 min before returning to ice. RT reaction mix (2.85 µl; final concentration 1µM template-switching oligo, 1× Maxima RT buffer (Life Technologies), 1 M betaine, 5 mM dithiothreitol, 6 mM $MgCl_2$, 0.5 U SUPERase RNase inhibitor, 2 U Maxima RT) was added and the plate was incubated in a Thermomixer C with ThermoTop (Eppendorf) (42 °C for 2 min at 2,000 r.p.m.; 42 °C for 60 min at 1,500 r.p.m.; 50 °C for 30 min at 1,500 r.p.m.; 60 °C for 10 min at 1,500 r.p.m.) or in a thermocycler (42 °C for 90 min, followed by 10 cycles of 50 °C for 2 min and 42 °C for 2 min, then 70 °C for 15 min) . After the RT reaction, 7.5 µl of pre-amp PCR mix (final concentration 1× KAPA HiFi HotStart Readymix (Kapa Biosystems), 0.1 µM IS PCR primer) was added to each well, and the plate was incubated in a thermocycler: 3 min at 98 °C, (cycle no.) × (98 °C for 20 s, 67 °C for 15 s, 72 °C for 6 min), 72 °C for 5 min. The number of preamplification cycles varied between 18 and 21 but had little effect on final library quality or complexity. Full-length cDNA was cleaned up using a 0.8× Ampure XP protocol (Beckman Coulter). Final libraries were built from successful cDNA preps using the Nextera XT kit (Illumina) with reduced volume (one-quarter or one-fifth standard volumes). Positive control samples from the first part of the protocol were replaced with water (no DNA controls) before performing Nextera prep. Up to 384 libraries were multiplexed together and sequenced on an Illumina HiSeq 2000 using a 40-bp single-end protocol, or on an Illumina NextSeq using a 40×40 bp paired-end protocol. All libraries are listed in Supplementary Data 1.

Primer sequences were as follows:
oligo(dT): /5BiosG/AAGCAGTGGTATCAACGCAGAGTACTTTTTTTTTTTTTTTTTTTTTTTTTTTTTTVN
Template-switching oligo (TSO): /5Biosg/AAGCAGTGGTATCAACGCAGAGTACATrGrG+G
IS PCR primer: /5BiosG/AAGCAGTGGTATCAACGCAGAGT

snRNA-seq data processing. Reads were trimmed and quality-filtered using Trim Galore v.0.4.1 (ref. [35]) and aligned using STAR v.2.7.1a[36]. To minimize mapping bias in favour of the reference strain (Col), reads from Col–Cvi crosses were mapped to a Col–Cvi 'metagenome', consisting of the TAIR10 sequence appended to a Cvi 'pseudogenome' generated by substituting the Cvi allele at 576,697 Col–Cvi single nucleotide polymorphisms (SNPs)[20]. Similarly, reads from Col–L*er* crosses were mapped to a Col–L*er* 'metagenome' created using 382,686 L*er* SNPs. Sequences from External RNA Controls Consortium (ERCC) RNA spike-ins (Thermo Fisher) were appended to the metagenome. Reads mapping uniquely to the ERCC sequences were omitted from the rest of the analysis. Reads with a single best alignment to the Col–Cvi or Col–L*er* metagenomes or with exactly two equal best alignments, each to equivalent positions on the Col and Cvi/L*er* chromosomes, were considered uniquely mapping. Procedures and scripts for mapping with the metagenome are available in ref. [37]. Reads overlapping an SNP were identified explicitly using a custom script (assign_to_allele.py, ref. [37]) and assigned to parent-of-origin. All SNPs within a read had to agree on parent-of-origin for the read to be considered allele-specific. PCR duplicates were removed using MarkDuplicates from the Picard Toolkit[38]. Total and allele-specific counts over genes were obtained using htseq-count v.0.9.1 (ref. [39]) and the Araport11 gene annotations (excluding new Araport11 annotations antisense to existing TAIR10 genes)[40]. Single-nuclei samples with a total of at least 1,500 genes detected (one or more overlapping read) and 1,000 genes well-detected (five or more overlapping reads) were considered high quality and kept for subsequent analyses. All negative controls (no nucleus sorted) lacked reads mapping to *Arabidopsis* (Supplementary Fig. 1). Despite arising from nuclear RNA, few intronic reads were recovered, although somewhat more than for whole-cell bulk mRNA-seq (Supplementary Fig. 2).

SC3 clustering and tissue assignment. Initial clustering of the full-count matrix was performed using SC3 (ref. [11]); a custom wrapper script used for these analyses (single_cell_cluster_SC3.R) is in the Github repository. Genes expressed in fewer than five nuclei or with fewer than ten total reads across all nuclei were omitted from this analysis, with a final set of 22,950 genes used for clustering. Counts were converted to counts per million (CPM) using the calculateCPM() function in the R package scater[41] before clustering. Optimal number of clusters was estimated using SC3's built-in algorithm. Benchmarking studies have found that SC3 tends to under-cluster[42]; we therefore sometimes performed additional sub-clustering on clusters that clearly contained additional subgroups (Fig. 1, Extended Data Figs. 2 and 3 and Supplementary Fig. 7).

Initial tissue assignments were made based on both the overall percentage of maternal reads detected for each nucleus (%mat), and a preliminary clustering using *t*-distributed Stochastic Neighbor Embedding (*t*-SNE) that strongly separated seed-coat and endosperm nuclei. *t*-SNE of all nuclei was performed on CPM values using the runTSNE() function in the scater package[41], and projected nuclei were clustered using *k*-means clustering with $k=3$. One of these clusters clearly corresponded to seed-coat nuclei based on %mat. Nuclei either in that cluster or with %mat > 85% were preliminarily assigned to seed coat, whereas those with %mat < 60% were preliminarily assigned to embryo, and all others were assigned to endosperm. Initial tissue assignments were refined based on the SC3 clusters, such that all nuclei in the same cluster were assigned to the tissue assignment of the majority of nuclei. Only 31 of 1,437 nuclei (2.16%) had their tissue assignments adjusted based on the SC3 clustering results.

At earlier stages of seed development, seeds contain few endosperm-derived 3C and 6C nuclei relative to diploid-derived nuclei (predominantly seed coat), and 3C/6C nuclei become difficult to sort accurately, particularly for very young (2–3 DAP) seeds (Extended Data Fig. 1). The 3C population is also generally smaller than the 6C population at early time points (2–4 DAP), but becomes larger at later time points (5 DAP). Because of these factors, seed-coat nuclei were obtained at varying rates, ranging from 0% to > 80% per batch/plate, with higher seed-coat recovery at earlier time points and when sorting from the 3C peak compared with the 6C peak (Extended Data Fig. 1).

After nuclei were assigned to specific tissues, SC3 was used to cluster nuclei from 4 DAP CxV and VxC F_1 endosperm and seed coat separately (Fig. 1b and Extended Data Fig. 3). For CxV endosperm, the 42 nuclei in the last cluster (cluster 10) were reclustered using SC3 to further resolve cell types. After comparing the results with the whole data set SC3 clustering (Extended Data Fig. 2), we further separated one of these clusters into clusters 12 and 13 manually, based on the fact that these were in two separate clusters in the full SC3 clustering and likely failed to be separated here because of the smaller number of nuclei. For VxC endosperm, initial clustering produced eight clusters, A–H. Cluster C ($n=30$) was reclustered into clusters 3 and 4, whereas clusters F–H ($n=208$) were not well-resolved and were also reclustered into clusters 7–11. For CxV seed coat, SC3 produced six clusters and no additional sub-clustering was performed. For VxC seed coat, the last cluster in the initial clustering was further subclustered into two clusters.

Identifying differentially expressed genes. Genes differentially expressed between clusters were identified using DESingle, which performs well with small numbers of cells[43,44]. See Supplementary Material.

Calculating expression enrichment scores and *P* values for gene-expression enrichment/depletion in particular clusters or across other factors. Gene expression enrichment scores (ES), which reflect the degree to which a gene's expression is enriched/depleted in a specific cluster relative to other clusters, were calculated using a custom script (cluster_gene_expression.R) available in the Github repository. This script uses permutation tests to estimate the degree to which a gene is specifically upregulated/downregulated in a cluster, and to calculate a *P* value for the significance of this enrichment in each cluster. Briefly, $\log_2$(CPM) values for each gene in each nucleus were averaged across all nuclei in each cluster. Cluster labels were then randomly permuted 1,000 times (controlling for various factors, see below), and average $\log_2$(CPM) values were calculated using the shuffled cluster labels for each permutation, yielding a background distribution of 1,000 values for each gene+cluster combination. Where applicable, we controlled for tissue type (endosperm versus seed coat), genotype (CxV versus VxC) and wash (yes/no indicating if nucleus was washed during preparation) by only permuting cluster labels among nuclei with the same tissue/genotype/wash. The mean and standard deviation of the $n=1{,}000$ permuted values was used to calculate a pseudo-*z*-score, called the 'enrichment score', reflecting the degree to which the true observed value x for any given gene/cluster combination is extreme relative to the random distribution estimated by permuting the cluster labels:

$$Z = \frac{x - \mu_B}{\sigma_B}$$

where μ_B and σ_B are the mean and standard deviation of the $n=1{,}000$ shuffled values, respectively. 'Enrichment score' matrices were clustered using either *k*-means clustering (Supplementary Fig. 4) or hierarchical clustering (Fig. 3a,d). The analysis proceeded similarly for calculating ESs over cell-cycle phases, with cell-cycle phase taking the place of clusters. Similarly, ES and *P* values over tissue/genotype/wash, where applicable, were also calculated by permuting the labels for tissue/genotype/wash across the different samples, and estimating pseudo-*z*-scores and *P* values as above. For example, to calculate ESs for genotype, which only has two values (CxV or VxC), CxV and VxC labels for all nuclei are shuffled 1,000 times and average values calculated for both categories each time. The degree to which average expression across the 'true' CxV labels deviates from the 1,000 randomly obtained values (represented as a *z*-score) is the ES. Because some of these variables have only two categories (for example, CxV or VxC) and the number of nuclei in each category is often similar, the resulting ESs tend to be symmetric around zero.

This analysis was performed using either total expression (Fig. 3a and Supplementary Fig. 4) or allelic expression (Fig. 3b). For allelic expression, the analysis described above was carried out over the maternal and paternal expression data separately (cluster_gene_expression.R-method separate), and the difference between the maternal and paternal ESs was plotted as a heatmap (Fig. 3b).

To estimate the probability that a gene's expression was enriched or depleted in a particular cluster, a *P* value equal to the fraction of times (out of 1,000 permutations) that the observed value x was greater than the shuffled mean was also calculated. If this value was less than 0.025, a gene was considered significantly depleted in that cluster; if the value was greater than 0.975, the gene was considered significantly enriched in that cluster.

GO term analysis. The R package 'topGO' was used to identify GO terms significantly enriched among certain groups of DE genes[45]. Briefly, GO annotations were obtained from plants_mart at plants.ensembl.org using the 'biomaRt' package[46]. Gene lists of interest were analysed using the topGO runTest function, with algorithm = 'elim' and statistic = 'fisher'. The background set of genes (gene universe) was the set of 29,428 genes with detectable expression in the full data set. For each gene list, all significant GO terms ($P < 0.005$) were obtained (Supplementary Data 2). The list of all genes associated with each GO term was obtained using the topGO genesInTerm() function. For plots showing average expression ESs for GO term-associated genes (Extended Data Figs. 4 and 5), ESs for all gene associated with each GO term were averaged together. A script for performing this analysis, run_topGO.R, is in the Github repository.

Cell-cycle analysis. To evaluate the positioning of our single-nuclei samples relative to the cell cycle, we performed a modified 'trajectory analysis' using a custom R script (single_cell_trajectory_analysis.R), available in the Github repository (Supplementary Material).

Identifying imprinted genes from snRNA-seq data. Assessing imprinting using snRNA-seq data is complicated by several factors, including dropouts (genes

not detected in a cell due to low input and technical factors) and transcriptional bursting kinetics, which can cause transcription at a locus to appear monoallelic at the moment of cell/nucleus capture even if a gene is expressed biallelically[47–49]. As a result, imprinting must be assessed by aggregating information from multiple single nuclei across the data set. Additionally, in most angiosperms including *Arabidopsis*, endosperm has a maternal:paternal (m:p) genome dosage of 2m:1p rather than 1m:1p. mRNAs from the two maternal alleles are indistinguishable, and thus cannot be modelled independently or directly compared with paternal expression, as in existing methods for assessing biased allelic expression from scRNA-seq[50,51]. We therefore developed a method for assessing imprinting that accounts for maternal and paternal dosage in endosperm (single_cell_ASE_analysis.R, Github repository) (Supplementary Material).

Reporting Summary. Further information on research design is available in the Nature Research Reporting Summary linked to this article.

Data availability

All sequencing data generated in this study have been deposited to the NCBI Gene Expression Omnibus with accession number GSE157145.

Code availability

Scripts used in analysis have been deposited to Github at https://github.com/clp90/endosperm_snRNAseq_2021.

Received: 4 December 2020; Accepted: 15 April 2021;
Published online: 31 May 2021

References

1. Li, J. & Berger, F. Endosperm: food for humankind and fodder for scientific discoveries. *New Phytol.* **195**, 290–305 (2012).
2. Gehring, M. & Satyaki, P. R. Endosperm and imprinting, inextricably linked. *Plant Physiol.* **173**, 143–154 (2017).
3. Costa, L. M., Gutièrrez-Marcos, J. F. & Dickinson, H. G. More than a yolk: the short life and complex times of the plant endosperm. *Trends Plant Sci.* **9**, 507–514 (2004).
4. Nguyen, H., Brown, R. C. & Lemmon, B. E. The specialized chalazal endosperm in *Arabidopsis thaliana* and *Lepidium verginicum* (Brassicaceae). *Protoplasma* **212**, 99–110 (2000).
5. Mansfield, S. G. & Briarty, L. G. Development of the free-nuclear endosperm in *Arabidopsis thaliana*. *Arabid. Inf. Serv.* **27**, 53–64 (1990).
6. Brown, R. C., Lemmon, B. E., Nguyen, H. & Olsen, O.-A. Development of endosperm in *Arabidopsis thaliana*. *Sex. Plant Reprod.* **12**, 32–42 (1999).
7. Brown, R. C., Lemmon, B. E. & Nguyen, H. Events during the first four rounds of mitosis establish three developmental domains in the syncytial endosperm of *Arabidopsis thaliana*. *Protoplasma* **222**, 167–174 (2003).
8. Boisnard-Lorig, C. et al. Dynamic analyses of the expression of the HISTONE::YFP fusion protein in *Arabidopsis* show that syncytial endosperm is divided in mitotic domains. *Plant Cell* **13**, 495–509 (2001).
9. Belmonte, M. F. et al. Comprehensive developmental profiles of gene activity in regions and subregions of the *Arabidopsis* seed. *Proc. Natl Acad. Sci. USA* **110**, E435–E444 (2013).
10. Picelli, S. et al. Smart-seq2 for sensitive full-length transcriptome profiling in single cells. *Nat. Methods* **10**, 1096–1098 (2013).
11. Kiselev, V. Y. et al. SC3: consensus clustering of single-cell RNA-seq data. *Nat. Methods* **14**, 483–486 (2017).
12. Radchuk, V. & Borisjuk, L. Physical, metabolic and developmental functions of the seed coat. *Front. Plant Sci.* **5**, 510 (2014).
13. Kiyosue, T. et al. Control of fertilization-independent endosperm development by the *MEDEA* polycomb gene in *Arabidopsis*. *Proc. Natl Acad. Sci. USA* **96**, 4186–4191 (1999).
14. Olsen, O. Nuclear endosperm development in cereals and *Arabidopsis thaliana*. *Plant Cell* **16**, S214–S227 (2004).
15. Baroux, C., Fransz, P. & Grossniklaus, U. Nuclear fusions contribute to polyploidization of the gigantic nuclei in the chalazal endosperm of *Arabidopsis*. *Planta* **220**, 38–46 (2004).
16. Alvarez-Buylla, E. R. et al. MADS-box gene evolution beyond flowers: expression in pollen, endosperm, guard cells, roots and trichomes. *Plant J.* **24**, 457–466 (2000).
17. Sørensen, M. B., Chaudhury, A. M., Robert, H., Bancharel, E. & Berger, F. Polycomb group genes control pattern formation in plant seed. *Curr. Biol.* **11**, 277–281 (2001).
18. Gorelova, V., Ambach, L., Rébeillé, F., Stove, C. & Van Der Straeten, D. Folates in plants: research advances and progress in crop biofortification. *Front. Chem.* **5**, 21 (2017).
19. Waters, A. J. et al. Comprehensive analysis of imprinted genes in maize reveals allelic variation for imprinting and limited conservation with other species. *Proc. Natl Acad. Sci. USA* **110**, 19639–19644 (2013).
20. Pignatta, D. et al. Natural epigenetic polymorphisms lead to intraspecific variation in *Arabidopsis* gene imprinting. *eLife* **3**, e03198 (2014).
21. Klosinska, M., Picard, C. L. & Gehring, M. Conserved imprinting associated with unique epigenetic signatures in the *Arabidopsis* genus. *Nat. Plants* **2**, 16145 (2016).
22. Hatorangan, M. R., Laenen, B., Steige, K. A., Slotte, T. & Köhler, C. Rapid evolution of genomic imprinting in two species of the Brassicaceae. *Plant Cell* **28**, 1815–1827 (2016).
23. Florez-Rueda, A. M. et al. Genomic imprinting in the endosperm is systematically perturbed in abortive hybrid tomato seeds. *Mol. Biol. Evol.* **33**, 2935–2946 (2016).
24. Liu, J. et al. Genome-wide screening and analysis of imprinted genes in rapeseed (*Brassica napus* L.) endosperm. *DNA Res.* **25**, 629–640 (2018).
25. Gehring, M. et al. DEMETER DNA glycosylase establishes *MEDEA* polycomb gene self-imprinting by allele-specific demethylation. *Cell* **124**, 495–506 (2006).
26. Satyaki, P. R. V. & Gehring, M. DNA methylation and imprinting in plants: machinery and mechanisms. *Crit. Rev. Biochem. Mol. Biol.* **52**, 163–175 (2017).
27. Batista, R. A. & Köhler, C. Genomic imprinting in plants – revisiting existing models. *Genes Dev.* **34**, 24–36 (2020).
28. Borg, M. et al. Targeted reprogramming of H3K27me3 resets epigenetic memory in plant paternal chromatin. *Nat. Cell Biol.* **22**, 621–629 (2020).
29. Haig, D. & Westoby, M. Parent-specific gene-expression and the triploid endosperm. *Am. Nat.* **134**, 147–155 (1989).
30. Patten, M. M. et al. The evolution of genomic imprinting: theories, predictions and empirical tests. *Heredity* **113**, 119–128 (2014).
31. Kunieda, T. et al. NAC family proteins NARS1/NAC2 and NARS2/NAM in the outer integument regulate embryogenesis in *Arabidopsis*. *Plant Cell* **20**, 2631–2642 (2008).
32. Jackson, D. in *Molecular Plant Pathology: A Practical Approach* (eds Gurr, S. J. et al.) 163–174 (Oxford Univ. Press, 1992).
33. Bortiri, E. et al. *ramosa2* encodes a LATERAL ORGAN BOUNDARY domain protein that determines the fate of stem cells in branch meristems of maize. *Plant Cell* **18**, 574–585 (2006).
34. Slane, D., Kong, J., Schmid, M., Jürgens, G. & Bayer, M. Profiling of embryonic nuclear vs. cellular RNA in *Arabidopsis thaliana*. *Genom. Data* **4**, 96–98 (2015).
35. Krueger, F. Trim-Galore. *Github* https://github.com/FelixKrueger/TrimGalore (2019).
36. Dobin, A. et al. STAR: ultrafast universal RNA-seq aligner. *Bioinformatics* **29**, 15–21 (2012).
37. Picard, C. L. & Gehring, M. in *Plant Epigenetics and Epigenomics: Methods and Protocols* (eds Spillane, C. & McKeown, P) 173–201 (Humana, 2020).
38. Picard Toolkit (Broad Institute, 2019); http://broadinstitute.github.io/picard
39. Anders, S., Pyl, T. P. & Huber, W. HTSeq—a Python framework to work with high-throughput sequencing data. *Bioinformatics* **31**, 166–169 (2015).
40. Cheng, C.-Y. et al. Araport11: a complete reannotation of the *Arabidopsis thaliana* reference genome. *Plant J.* **89**, 789–804 (2017).
41. McCarthy, D. J., Campbell, K. R., Lun, A. T. L. & Willis, Q. F. Scater: pre-processing, quality control, normalisation and visualisation of single-cell RNA-seq data in R. *Bioinformatics* **33**, 1179–1186 (2017).
42. Tian, L. et al. Benchmarking single cell RNA-sequencing analysis pipelines using mixture control experiments. *Nat. Methods* **16**, 479–487 (2019).
43. Miao, Z., Deng, K., Wang, X. & Zhang, X. DEsingle for detecting three types of differential expression in single-cell RNA-seq data. *Bioinformatics* **34**, 3223–3224 (2018).
44. Wang, T., Li, B., Nelson, C. E. & Nabavi, S. Comparative analysis of differential gene expression analysis tools for single-cell RNA sequencing data. *BMC Bioinform.* **20**, 40 (2019).
45. Alexa, A. & Rahnenfuhrer, J. topGO: Enrichment analysis for gene ontology. R package v. 2.40.0 (2020).
46. Durinck, S. et al. BioMart and Bioconductor: a powerful link between biological databases and microarray data analysis. *Bioinformatics* **21**, 3439–3440 (2005).
47. Kim, J. K., Kolodziejczyk, A. A., Illicic, T., Teichmann, S. A. & Marioni, J. C. Characterizing noise structure in single-cell RNA-seq distinguishes genuine from technical stochastic allelic expression. *Nat. Commun.* **6**, 8687 (2015).
48. Deng, Q., Ramsköld, D., Reinius, B. & Sandberg, R. Single-cell RNA-seq reveals dynamic, random monoallelic gene expression in mammalian cells. *Science* **343**, 193–196 (2014).
49. Borel, C. et al. Biased allelic expression in human primary fibroblast single cells. *Am. J. Hum. Genet.* **96**, 70–80 (2015).
50. Jiang, Y., Zhang, N. R. & Li, M. SCALE: modeling allele-specific gene expression by single-cell RNA sequencing. *Genome Biol.* **18**, 74 (2017).
51. Choi, K., Raghupathy, N. & Churchill, G. A. A Bayesian mixture model for the analysis of allelic expression in single cells. *Nat. Commun.* **10**, 5188 (2019).

52. Schon, M. A. & Nodine, M. D. Widespread contamination of *Arabidopsis* embryo and endosperm transcriptome data sets. *Plant Cell* **29**, 608–617 (2017).
53. Hoffman, G. E. & Schadt, E. E. variancePartition: interpreting drivers of variation in complex gene expression studies. *BMC Bioinform.* **17**, 483 (2016).
54. Windsor, J. B., Symonds, V. V., Mendenhall, J. & Lloyd, A. M. *Arabidopsis* seed coat development: morphological differentiation of the outer integument. *Plant J.* **22**, 483–493 (2000).
55. Nakaune, S. et al. A vacuolar processing enzyme, deltaVPE, is involved in seed coat formation at the early stage of seed development. *Plant Cell* **17**, 876–887 (2005).
56. Mizzotti, C. et al. SEEDSTICK is a master regulator of development and metabolism in the *Arabidopsis* seed coat. *PLoS Genet.* **10**, e1004856 (2014).

Acknowledgements

We thank the Massachusetts Institute of Technology (MIT) BioMicro Center and the Whitehead Institute Genome Technology Core and Flow Cytometry Core Facility for research assistance, and F. Lafontaine for valuable input on statistical methods. This research was funded by NIH R01 GM112851 and NSF MCB 1453459 grants to M.G., NSF Graduate Research Fellowship and Abraham Siegel Fellowship to C.L.P., and NSF IOS 1812116 to R.A.P.

Author contributions

M.G. and C.L.P. conceived the project. C.L.P. and R.A.P. conducted experiments. C.L.P., R.A.P. and B.P.W. analysed data with input from M.G. C.L.P. and M.G. wrote the manuscript with edits from R.A.P and B.P.W.

Competing interests

The authors declare no competing interests.

Additional information

Extended data is available for this paper at https://doi.org/10.1038/s41477-021-00922-0.

Supplementary information The online version contains supplementary material available at https://doi.org/10.1038/s41477-021-00922-0.

Correspondence and requests for materials should be addressed to M.G.

Peer review information *Nature Plants* thanks the anonymous reviewers for their contribution to the peer review of this work.

Reprints and permissions information is available at www.nature.com/reprints.

Publisher's note Springer Nature remains neutral with regard to jurisdictional claims in published maps and institutional affiliations.

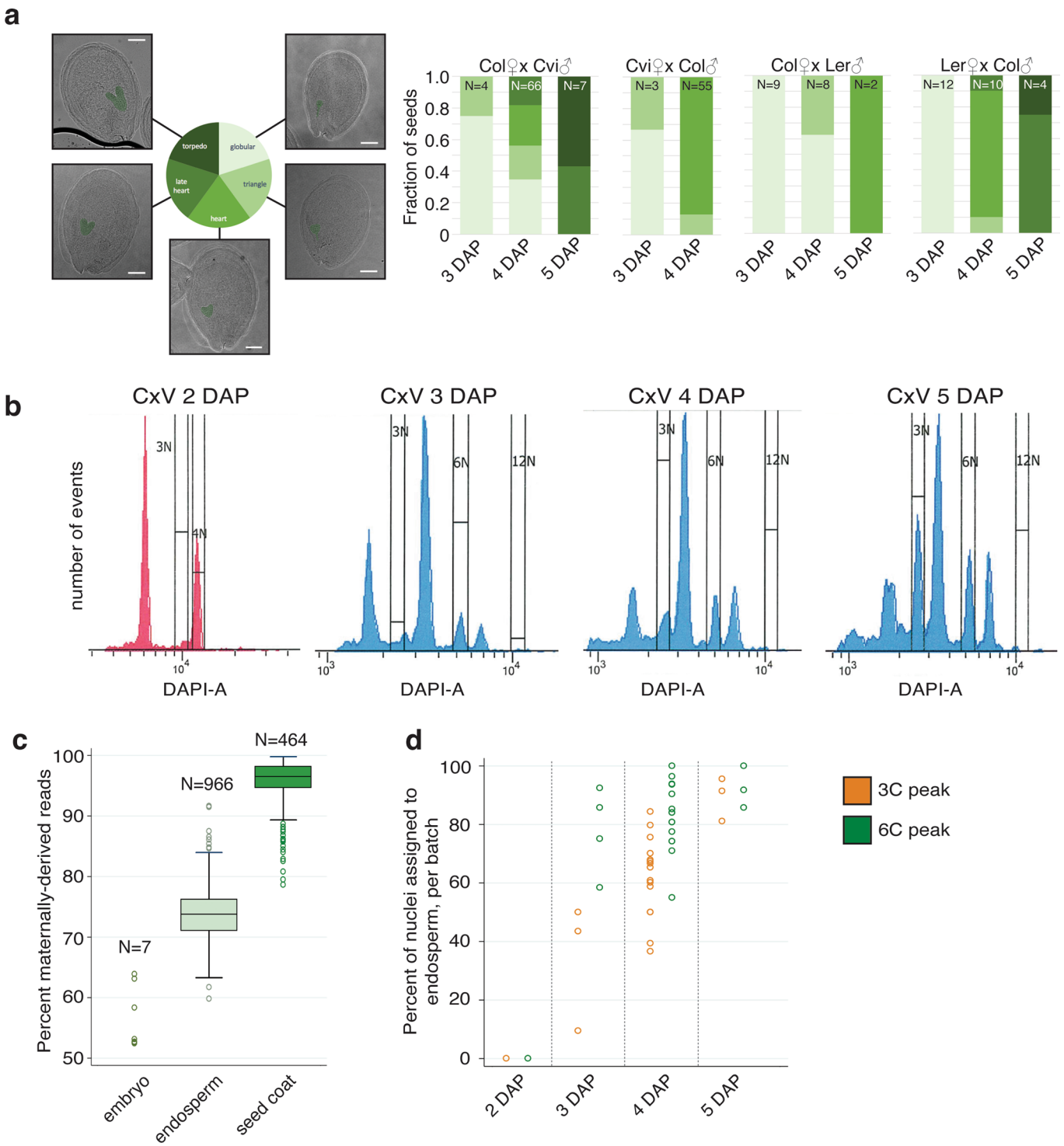

Extended Data Fig. 1 | Seed developmental stages assayed, FANS profiles, and impact on endosperm enrichment. (a) Summary of seed developmental stages in the different genotypes and timepoints assayed. Number of seeds imaged for each bar shown at top. Scale bar 100 µm. (b) FANS sorting profiles of Col x Cvi (CxV) seeds at 2 DAP (sorted 09/26/17), 3 DAP (08/10/17), 4 DAP (11/16/17) and 5 DAP (11/14/17). The 2 DAP sample was processed on a different FACS machine than the other three samples. (c) Percent of allelic reads that were derived from the maternally inherited allele, for nuclei assigned as embryo, endosperm, and seed coat (see methods). Median, interquartile range and upper-/lower-adjacent values (1.5*IQR) indicated by center line, box, and whiskers of each boxplot, respectively. (d) Percent of nuclei per batch (96-well plate) assigned to endosperm. Nuclei from later timepoints, as well as from the 6C peak, are more likely to correspond to endosperm than nuclei from earlier timepoints or from the 3C peak.

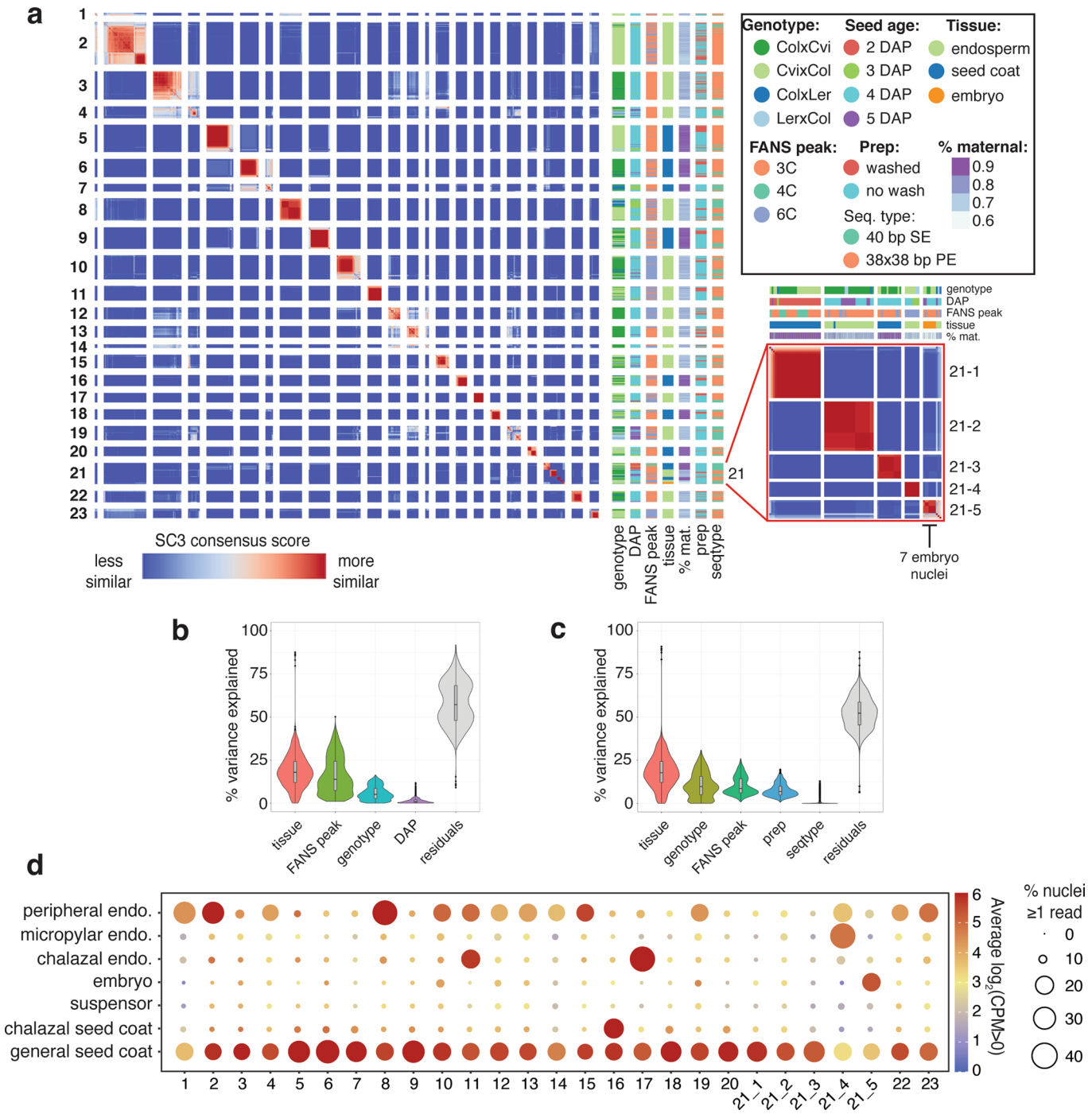

Extended Data Fig. 2 | Clustering of all 1437 high-quality nuclei in the dataset. (a) Heatmap of SC3 clustering of all 1437 nuclei. Genotype, FANS peak, prep method (see 'Seed nuclei FANS'), sequencing type, % maternal (percent of allelic reads derived from maternal allele), and seed age also shown. (b) Partitioning of the variance in CPM values for the 22,950 expressed genes in the dataset over the 1437 nuclei samples, according to tissue, peak, genotype and DAP, using the R package 'variancePartition'[53]. Median, interquartile range and upper-/lower-adjacent values (1.5*IQR) indicated by center line, box, and whiskers within each violin plot. (c) Same as (b), over the 1096 Col x Cvi and Cvi x Col 4 DAP samples only. In this group, prep and sequencing type are less confounded with sources of biological variation (for example all washed samples are either Col x Cvi or Cvi x Col 4 DAP, so prep is confounded with genotype and DAP in the full dataset), so their contribution to the variation could be more reliably estimated. (d) Average expression of marker genes for various seed compartments (globular and heart stage)[9,52] for nuclei in each cluster. Size indicates the average percent of nuclei with > 0 counts, color indicates average $\log_2$(CPM) for all nuclei with CPM > 0.

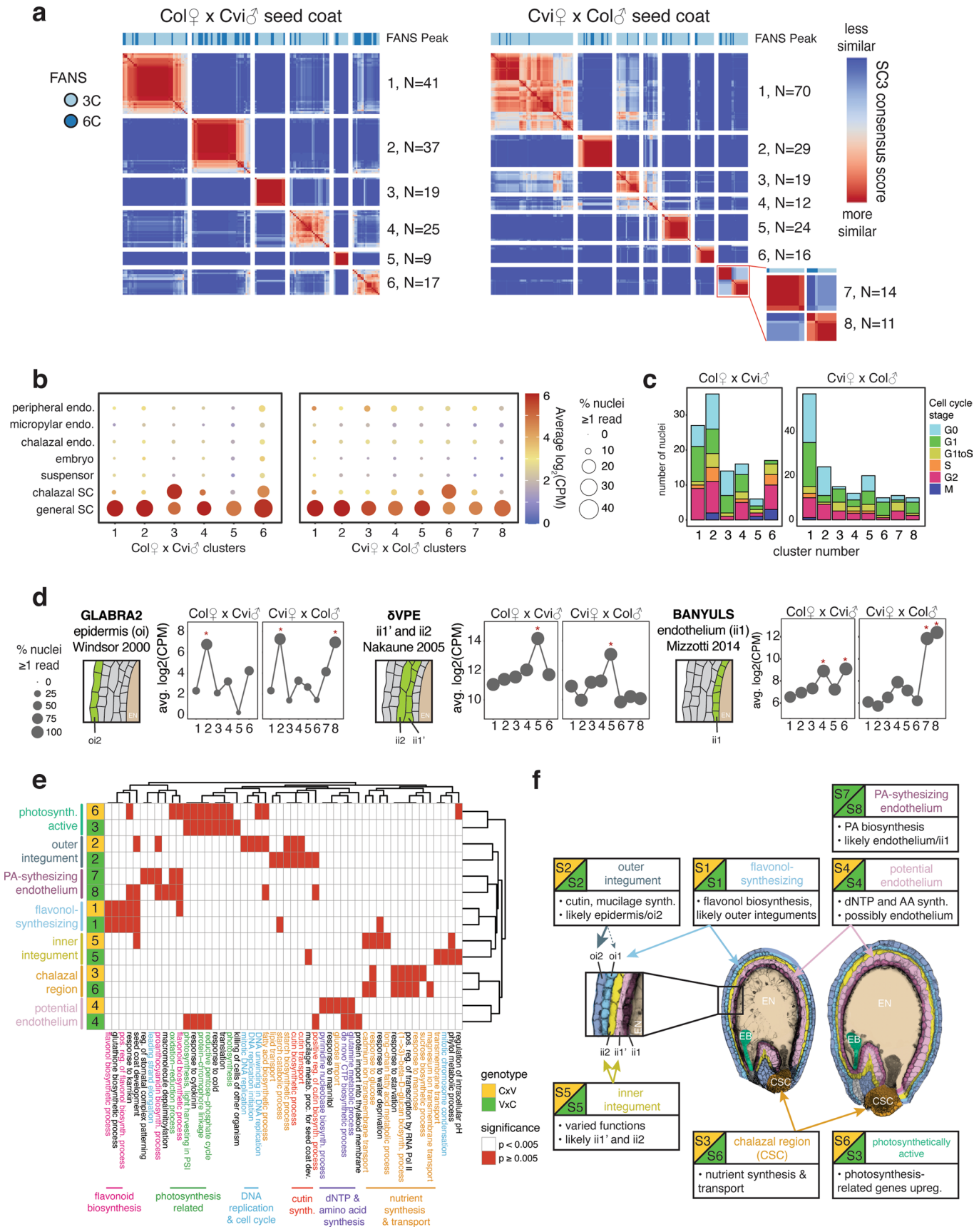

Extended Data Fig. 3 | See next page for caption.

Extended Data Fig. 3 | Characterization of seed coat nuclei. (a) SC3 clustering of 4 DAP seed coat nuclei. (b) Average expression of LCM seed tissue markers[9,52], over seed coat clusters. Dot color: average $\log_2$(CPM); dot size: average percent nuclei with CPM > 0. (c) Cell cycle phase by cluster. (d) Average expression of genes specific to particular seed coat cell layers[54–56] across nuclei clusters. Schematic of seed coat cell layers, from ii1 (the endothelium, innermost) to oi2 (epidermis, outermost); layers where expression was observed in indicated study highlighted green. Red star: significantly higher expression in cluster (permutation test, $p < 0.05$). (e) Top 5 GO terms for significantly upregulated genes in each cluster. (f) Cluster identities and characteristics; false-colored Col x Cvi (left) and Cvi x Col (right) seed images. EB = embryo, EN = endosperm, CSC = chalazal seed coat. Inset: the five seed coat cell layers.

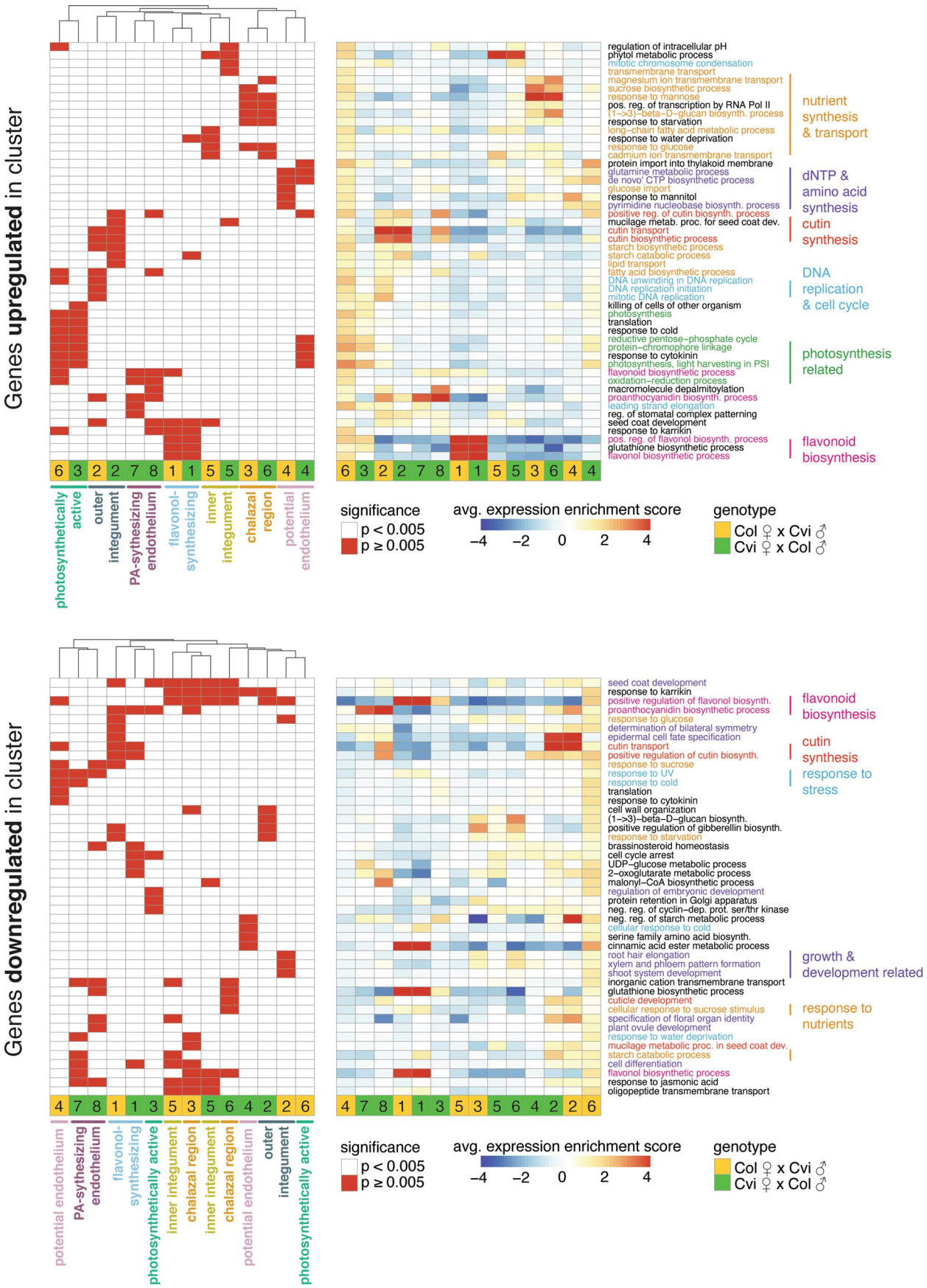

Extended Data Fig. 4 | See next page for caption.

Extended Data Fig. 4 | Heatmaps of the 5 most significantly enriched GO terms among genes upregulated (top) and downregulated (bottom) in each seed coat cluster. Significant terms are flagged in left heatmap, while average expression 'enrichment score' across all genes associated with GO term is shown at right. Average includes any genes associated with the GO-term that are not significantly up/downregulated in the indicated cluster, so average may not reflect expectations. Full lists of significant GO-terms, and specific lists of genes in each significant GO-term that are up/downregulated in cluster, are in Supplementary Data 2. Order of rows and columns same for left and right heatmaps.

Extended Data Fig. 5 | See next page for caption.

Extended Data Fig. 5 | Heatmaps of the 5 most significantly enriched GO terms among genes upregulated (top) and downregulated (bottom) in each endosperm cluster. Significant terms, $p < 0.005$, are flagged in left heatmap, while average expression 'enrichment score' across all genes associated with GO term is shown at right. Average includes any genes associated with the GO-term that are not significantly up/downregulated in the indicated cluster; so average may not reflect expectations. Full lists of significant GO-terms, and specific lists of genes in each significant GO-term that are up/downregulated in cluster, are in Supplementary Data 2. Order of rows/columns same for left and right heatmaps.

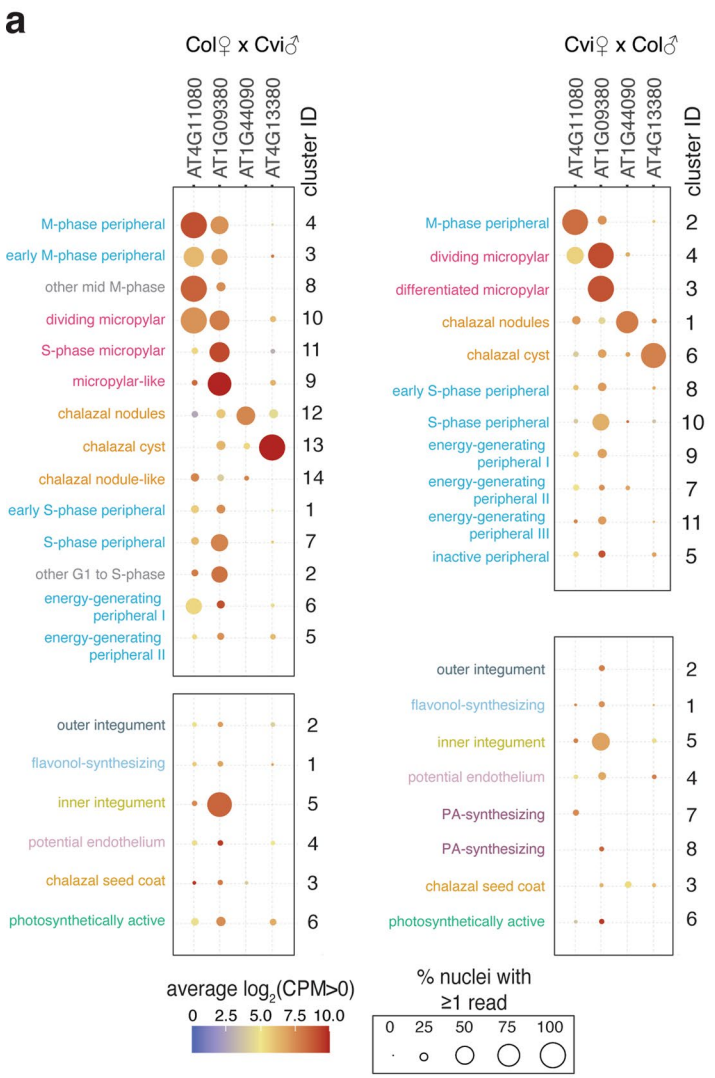

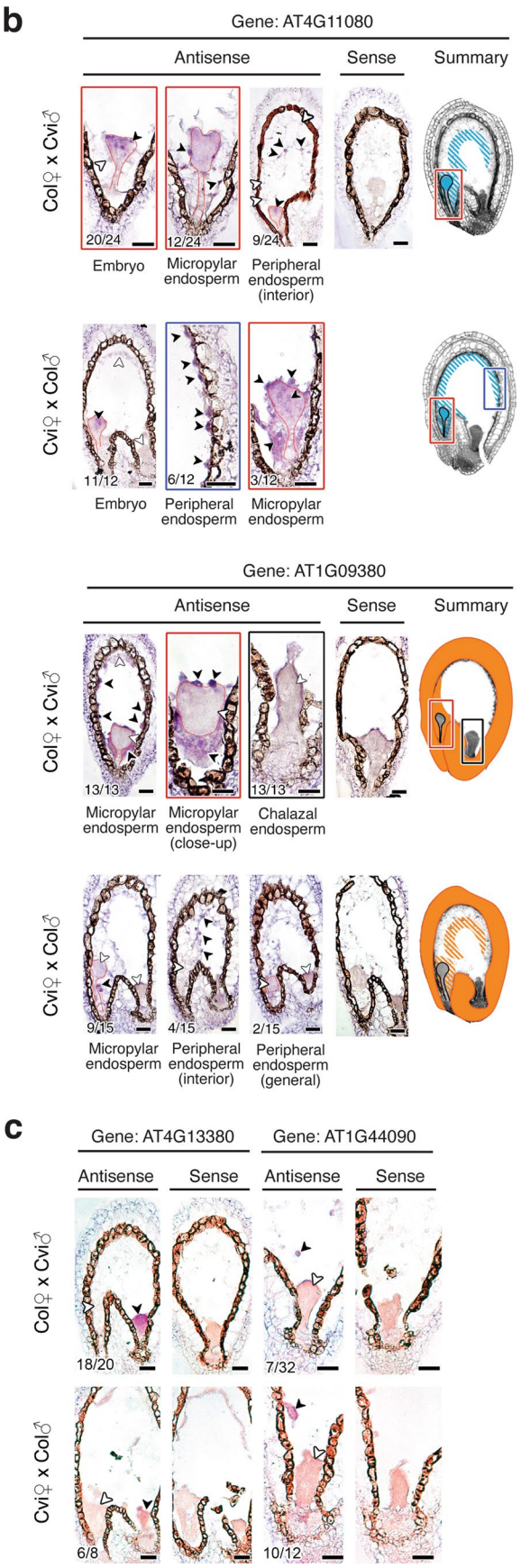

Extended Data Fig. 6 | See next page for caption.

Extended Data Fig. 6 | In situ hybridization analysis for additional cluster-specific transcripts. (a) Expression data for four additional marker genes used for RNA *in situ* hybridization experiments, across endosperm and seed coat clusters. (b) *In situ* hybridization (purple signal) results for two micropylar/peripheral clusters. AT4G11080 is most notably expressed in peripheral and micropylar endosperm and in the embryo. AT1G09380 is most notably expressed in the micropylar endosperm and seed coat. In gene summaries, expression indicated by hatched pattern indicates variable expression in that zone among seeds. (c) *In situ* hybridization results for two additional chalazal endosperm transcripts not shown in Fig. 2: AT4G13380 is predominantly expressed in the chalazal cyst, while AT1G44090 is predominantly expressed in the chalazal nodules. (b-c) Black arrowheads indicate sites of transcript accumulation; white arrowheads indicate examples of sites without transcripts. Number of seeds with expression in specific zones relative to the number of seeds examined is shown in bottom left of panels; expression in one zone does not exclude expression in other zones. Seeds were from three independent controlled pollination events, collected together. For all antisense probes, in situ experiment was performed at least twice, except for AT4G11080, which was performed once. Both sense and antisense probe images shown. Scale bars = 25 μm.

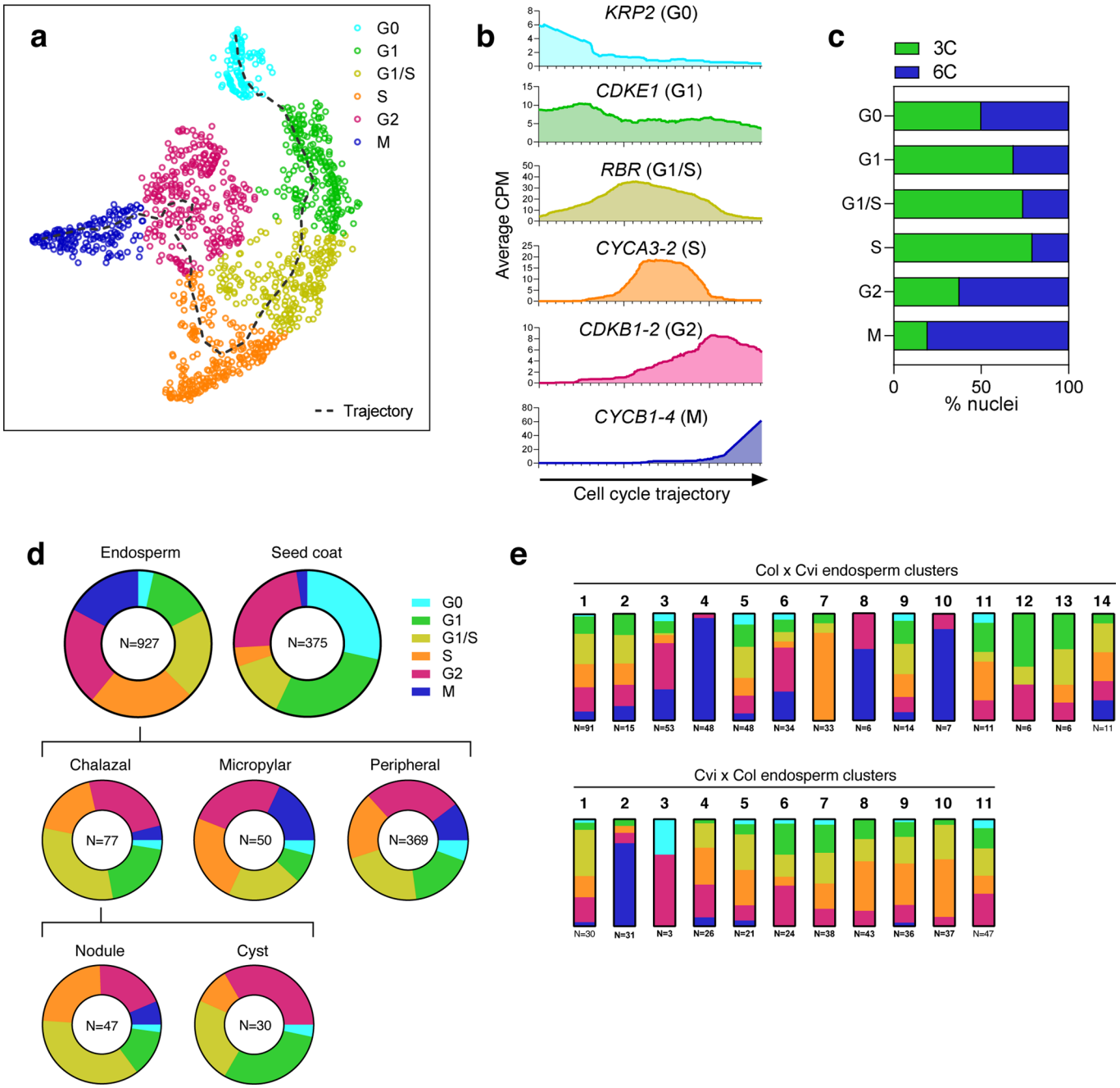

Extended Data Fig. 7 | Cell cycle is a source of variability among endosperm clusters. (a) t-SNE projection and trajectory analysis of 1,309 nuclei in the dataset, based on expression of a manually curated list of 22 cell cycle-dependent marker genes. Dotted line represents cell cycle trajectory from G0 -> G1 -> S -> G2 -> M. (b) Average expression of six of the 22 marker genes used in analysis shown in (a), with nuclei ordered according to their linear projection onto the cell cycle trajectory, starting from G0 (left) to M (right). Moving averages were calculated using a sliding window of 200 data points. (c) Percent of nuclei in each phase of the cell cycle that were sorted from the 3C or 6C FANS peak (d) Distribution of nuclei among cell cycle phases in seed coat and endosperm. Endosperm data are further divided into peripheral, micropylar, and chalazal; the chalazal region is also divided into the cyst and nodules. (e) Distribution of nuclei among cell cycle phases for each of the endosperm clusters.

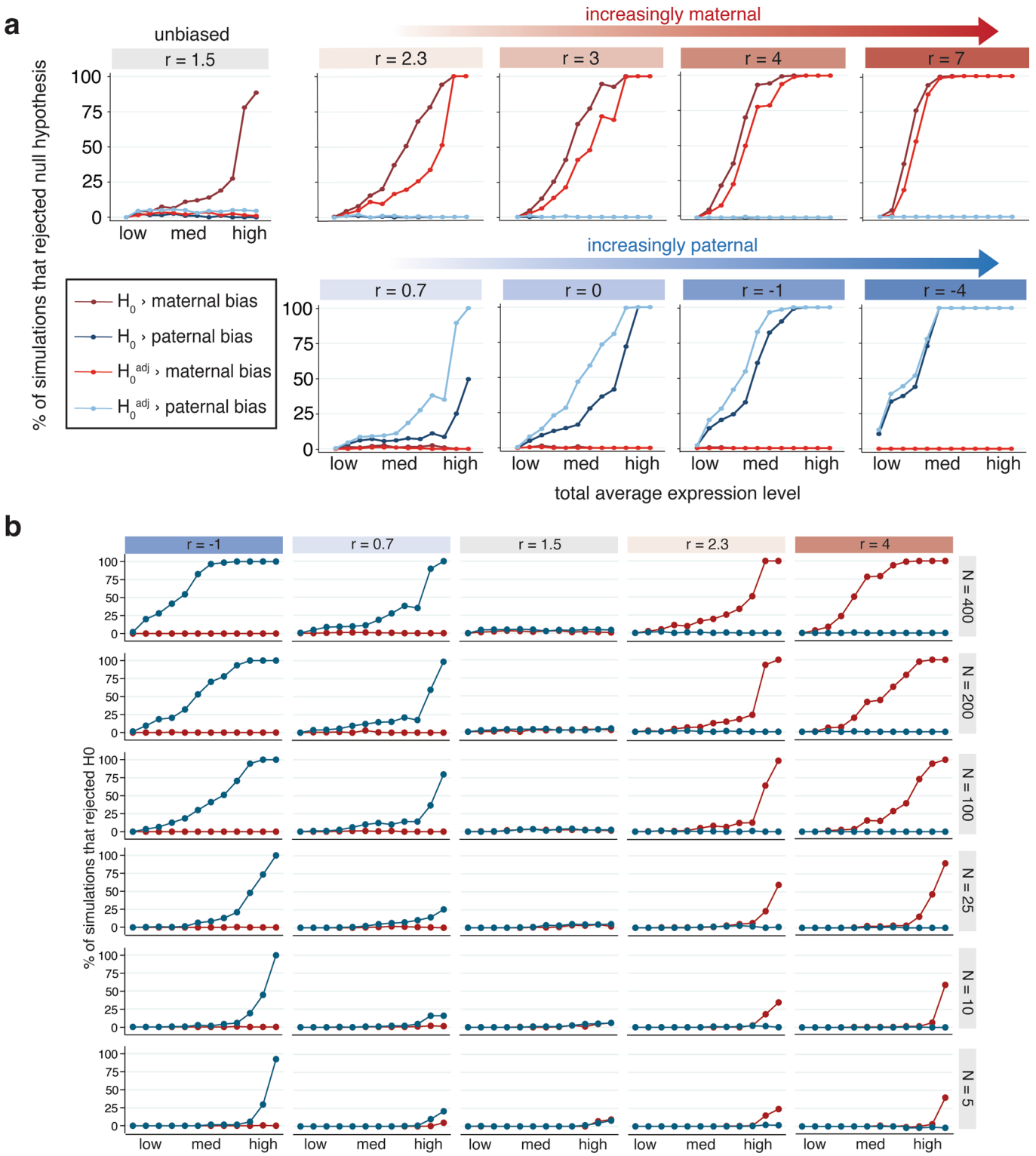

Extended Data Fig. 8 | Statistical power and accuracy of imprinting model under various simulated conditions. (a) Percent of simulations (out of 200) where the null hypothesis of no parental bias was rejected, for simulations with varied total expression and $\log_2$(m/p) ratio (r). Simulations mimicked degree of maternal skew in the Col x Cvi data, so 'unbiased' simulations had r = 1.5. Twelve values of total expression were tested: 0.01, 0.05, 0.1, 0.15, 0.25, 0.5, 0.75, 1.0, 1.5, 3.5, 15, and 50. The 1st, 25th, 50th, 75th and 99th percentiles for total expression in the Col x Cvi dataset are 0.033, 0.21, 0.58, 1.57 and 15.4, respectively. Blue lines indicate paternal bias, red indicate maternal bias. (b) Effect of number of observations (nuclei) in simulations on power to reject H_0^{adj}. Highly expressed and highly biased genes can be detected even with as few as 5 observations. Blue lines indicate tests for paternal bias, red indicate tests for maternal bias.

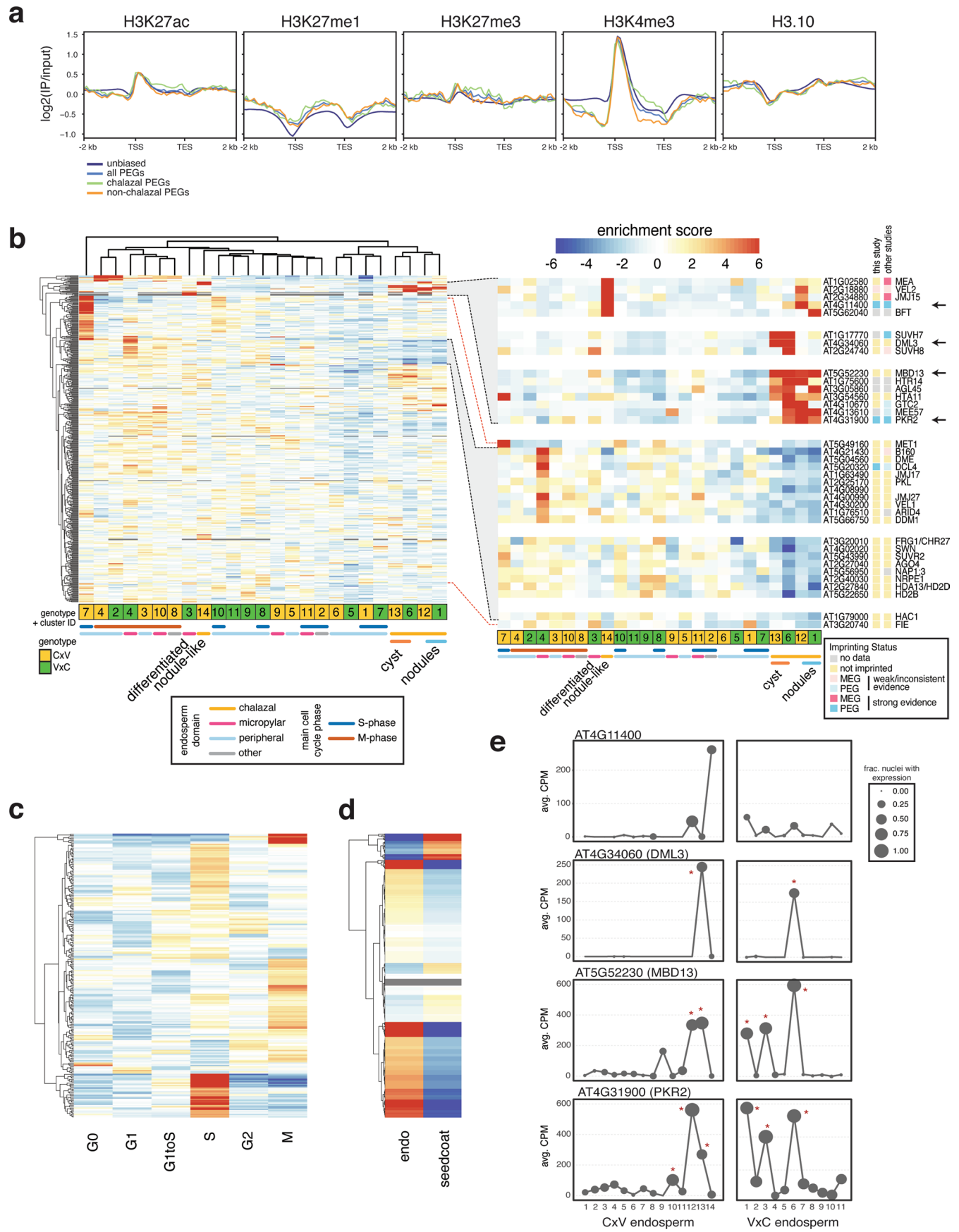

Extended Data Fig. 9 | See next page for caption.

Extended Data Fig. 9 | Expression of chromatin-related genes. (a) Sperm ChIP-seq profiles from[28] over non-imprinted genes, all PEGs, chalazal PEGs and non-chalazal PEGs. (b) Heatmap of expression enrichment scores (ES) across endosperm nuclei clusters, for 464 chromatin-related genes with variable expression across the clusters. Inset: subset of genes enriched in chalazal nodules, cyst, or both (top); subset of genes with depleted expression in chalazal endosperm, grouped by expression pattern (bottom). Not all genes in highlighted region in left plot shown. (c) Heatmap of expression ES for the full 4 DAP endosperm + seed coat dataset, over cell cycle phases. 227 chromatin-related genes with variation across cell cycle shown. Color bar same as (b). (d) Expression ES in endosperm vs. seed coat for 553 chromatin-related genes. Color bar same as (b). (e) Average expression profiles across the endosperm clusters for four genes shown in (b) (see arrows). Stars indicate clusters with significantly enriched expression based on a permutation test. CPM = counts per million.

nature research

Corresponding author(s): Mary Gehring

Last updated by author(s): Apr 6, 2021

Reporting Summary

Nature Research wishes to improve the reproducibility of the work that we publish. This form provides structure for consistency and transparency in reporting. For further information on Nature Research policies, see our Editorial Policies and the Editorial Policy Checklist.

Statistics

For all statistical analyses, confirm that the following items are present in the figure legend, table legend, main text, or Methods section.

n/a	Confirmed	
☐	☒	The exact sample size (*n*) for each experimental group/condition, given as a discrete number and unit of measurement
☒	☐	A statement on whether measurements were taken from distinct samples or whether the same sample was measured repeatedly
☐	☒	The statistical test(s) used AND whether they are one- or two-sided *Only common tests should be described solely by name; describe more complex techniques in the Methods section.*
☒	☐	A description of all covariates tested
☐	☒	A description of any assumptions or corrections, such as tests of normality and adjustment for multiple comparisons
☐	☒	A full description of the statistical parameters including central tendency (e.g. means) or other basic estimates (e.g. regression coefficient) AND variation (e.g. standard deviation) or associated estimates of uncertainty (e.g. confidence intervals)
☐	☒	For null hypothesis testing, the test statistic (e.g. *F*, *t*, *r*) with confidence intervals, effect sizes, degrees of freedom and *P* value noted *Give P values as exact values whenever suitable.*
☒	☐	For Bayesian analysis, information on the choice of priors and Markov chain Monte Carlo settings
☒	☐	For hierarchical and complex designs, identification of the appropriate level for tests and full reporting of outcomes
☐	☒	Estimates of effect sizes (e.g. Cohen's *d*, Pearson's *r*), indicating how they were calculated

Our web collection on statistics for biologists contains articles on many of the points above.

Software and code

Policy information about availability of computer code

Data collection	No software was used.
Data analysis	All custom code and scripts generated for this project can be accessed here: https://github.com/clp90/endosperm_snRNAseq_2021, along with detailed dependencies and other information. Other software used: BD FACSDiva v.8.0.1 Zen 2012 (blue edition) Adobe Photoshop 21.2.6 bedtools v.2.23.0 samtools v.1.9 python v.2.7.17 R v3.6.3 fastqc (0.11.8) Trim Galore v.0.5.0 STAR v.2.6.1d Java 1.8.0_191 MarkDuplicates v1.121 from picard toolkit deeptools v.3.2.0 R packages argparse (2.0.1), ggplot2 (3.3.2), RColorBrewer (1.1.2), viridis (0.5.1), pheatmap (1.0.12), dplyr (1.0.2), optparse (1.6.6), DEsingle (1.6.0), gplots (3.1.0), topGO (2.38.1), biomaRt (2.42.1), Rgraphviz (2.30.0), grid (3.6.3), gmodels (2.18.1), gamlss (5.2.0), VGAM (1.1.3), maxLik (1.4.4), metap (1.4), gridExtra (2.3), vcd (1.4.8), scater (1.14.6), fpc (2.2.8), princurve (2.1.5), SC3 (1.14.0), reshape2 (1.4.4), Rtsne (0.15), data.table (1.13.0), tidyr (1.1.2), igraph (1.2.6), maptools (1.0.2), spatstat (1.64.1), RANN (2.6.1), pscl (1.5.5), MASS (7.3.53), boot (1.3.25),

stats (3.6.3), edgeR (3.28.1), plyr (1.8.6)
Python packages argparse (1.1), numpy (1.15.1), cutadapt (1.18), HTSeq (0.11.0)

For manuscripts utilizing custom algorithms or software that are central to the research but not yet described in published literature, software must be made available to editors and reviewers. We strongly encourage code deposition in a community repository (e.g. GitHub). See the Nature Research guidelines for submitting code & software for further information.

Data

Policy information about availability of data

All manuscripts must include a data availability statement. This statement should provide the following information, where applicable:

- Accession codes, unique identifiers, or web links for publicly available datasets
- A list of figures that have associated raw data
- A description of any restrictions on data availability

All sequencing data generated in this study have been deposited to the Gene Expression Omnibus with accession number GSE157145, accessible at https://www.ncbi.nlm.nih.gov/geo/query/acc.cgi?acc=GSE157145

Field-specific reporting

Please select the one below that is the best fit for your research. If you are not sure, read the appropriate sections before making your selection.

☒ Life sciences ☐ Behavioural & social sciences ☐ Ecological, evolutionary & environmental sciences

For a reference copy of the document with all sections, see nature.com/documents/nr-reporting-summary-flat.pdf

Life sciences study design

All studies must disclose on these points even when the disclosure is negative.

Sample size	No sample size was chosen. Because a single seed has approximately 350 endosperm nuclei at 4 DAP, we ensured we sequenced at least twice that amount of endosperm nuclei.
Data exclusions	Data from single-nuclei sequencing that did not meet quality thresholds were not included in the analysis. Only single-nuclei samples with a total of at least 1,500 genes detected (≥ 1 overlapping read) and 1,000 genes well-detected (≥ 5 overlapping reads) were considered high quality and kept for subsequent analyses.
Replication	Single nuclei data were used to predict distinct nuclei types; these were verified experimentally using in situ hybridization of several marker genes unique to specific nuclei clusters. This confirmed that variation in nuclei types present in the data reflect real differences among endosperm nuclei.
Randomization	Not applicable - no treatment/control groups used.
Blinding	Not applicable - no treatment/control groups used.

Reporting for specific materials, systems and methods

We require information from authors about some types of materials, experimental systems and methods used in many studies. Here, indicate whether each material, system or method listed is relevant to your study. If you are not sure if a list item applies to your research, read the appropriate section before selecting a response.

Materials & experimental systems

n/a	Involved in the study
☐	☒ Antibodies
☒	☐ Eukaryotic cell lines
☒	☐ Palaeontology and archaeology
☒	☐ Animals and other organisms
☒	☐ Human research participants
☒	☐ Clinical data
☒	☐ Dual use research of concern

Methods

n/a	Involved in the study
☒	☐ ChIP-seq
☐	☒ Flow cytometry
☒	☐ MRI-based neuroimaging

Antibodies

Antibodies used	Anti-Digoxigenin-AP, Fab fragments (from sheep), Roche Diagnostics (Made in Mannheim, Germany), REF 11 093 274 910, LOT 11266027 (March 2018).

Validation	From manufacture's website: "Analysis Note: Cross reactivity to digitoxin and digitoxigenin: <1 %. No cross reactivity with other human estrogen or androgen steroids, e.g. estradiol or testosterone. Cross reactivity with digoxin: not known. Conjugate does not bind to itself at all. Normally one molecule of the conjugate binds to one molecule digoxigenin, although there are two possible binding sites for digoxigenin. Nonspecific binding to RNA is not expected." From experiments presented in paper: negative control treatments (sense probes using DIG-labeled nucleotides, which are not expected to bind to mRNAs present in tissue) did not produce identifiable/specific patterns of Anti-DIG binding to tissue.

Flow Cytometry

Plots

Confirm that:

☒ The axis labels state the marker and fluorochrome used (e.g. CD4-FITC).

☒ The axis scales are clearly visible. Include numbers along axes only for bottom left plot of group (a 'group' is an analysis of identical markers).

☒ All plots are contour plots with outliers or pseudocolor plots.

☒ A numerical value for number of cells or percentage (with statistics) is provided.

Methodology

Sample preparation	Seeds were manually removed from siliques (~ 2 siliques per sample) into 50 uL Partec nuclei extraction buffer + 6 uL SUPERase RNase inhibitor (20 U/uL). Samples were disrupted using a blue pestle in a microfuge tube before adding 400 uL Partec nuclei staining buffer and mixing by pipetting. Samples were filtered twice through a 30um nylon mesh (Partec CellTrics #04-004-2326, Sysmex). For samples sorted on 9/12/2018, 9/13/2018, 9/20/2018 and 9/26/2018, two additional wash steps were performed to potentially remove cell lysate from the sample (see Supplementary Data S1). For each wash, nuclei were spun down 5 min at 1000 g in a centrifuge pre-cooled to 4°C. Supernatant was then removed and nuclei were gently resuspended in 1 mL of a 1:8 mix of Partec nuclei extraction buffer and Partec nuclei staining buffer. Individual nuclei were sorted into wells of a 96-well PCR plate using a BD FACSAria II flow cytometer. A total of 22 full or partial plates (batches) of samples were prepared. Each plate included at least one negative control (no nucleus sorted into well) and one positive control (50 nuclei sorted into a single well); however, these controls were not sequenced in the first batch (Supplementary Data S1). Some plates also included wells with 2 nuclei sorted into each as controls for the precision of single-nuclei sorting.
Instrument	BD FACSAria II flow cytometer
Software	FACSDiva v.8.0.1
Cell population abundance	Final proportion of endosperm nuclei within sorted populations varied from 40-100% for 4 day after pollination (DAP) seeds (the bulk of the dataset). Contaminating nuclei were from seed coat. Variation was due to factors like ploidy peak sorted (more contamination from 3C than 6C peak), seed stage (no endosperm could be recovered at 2 DAP), etc.
Gating strategy	The population of droplets containing nuclei was first gated based on DNA content (DAPI-A) and size (FSC-A). For nuclei in this population, histogram of DAPI intensity (DAPI-A) showed clear peaks corresponding to various 2C-derived (seed coat) and 3C-derived (endosperm) nuclei. The 3C and 6C peaks were gated for sorting. Gating strategy is shown in Extended Data Fig. 1.

☒ Tick this box to confirm that a figure exemplifying the gating strategy is provided in the Supplementary Information.